Towards a mechanistic understanding of nanoparticle behavior using zebrafish

Arias Alpizar, G.

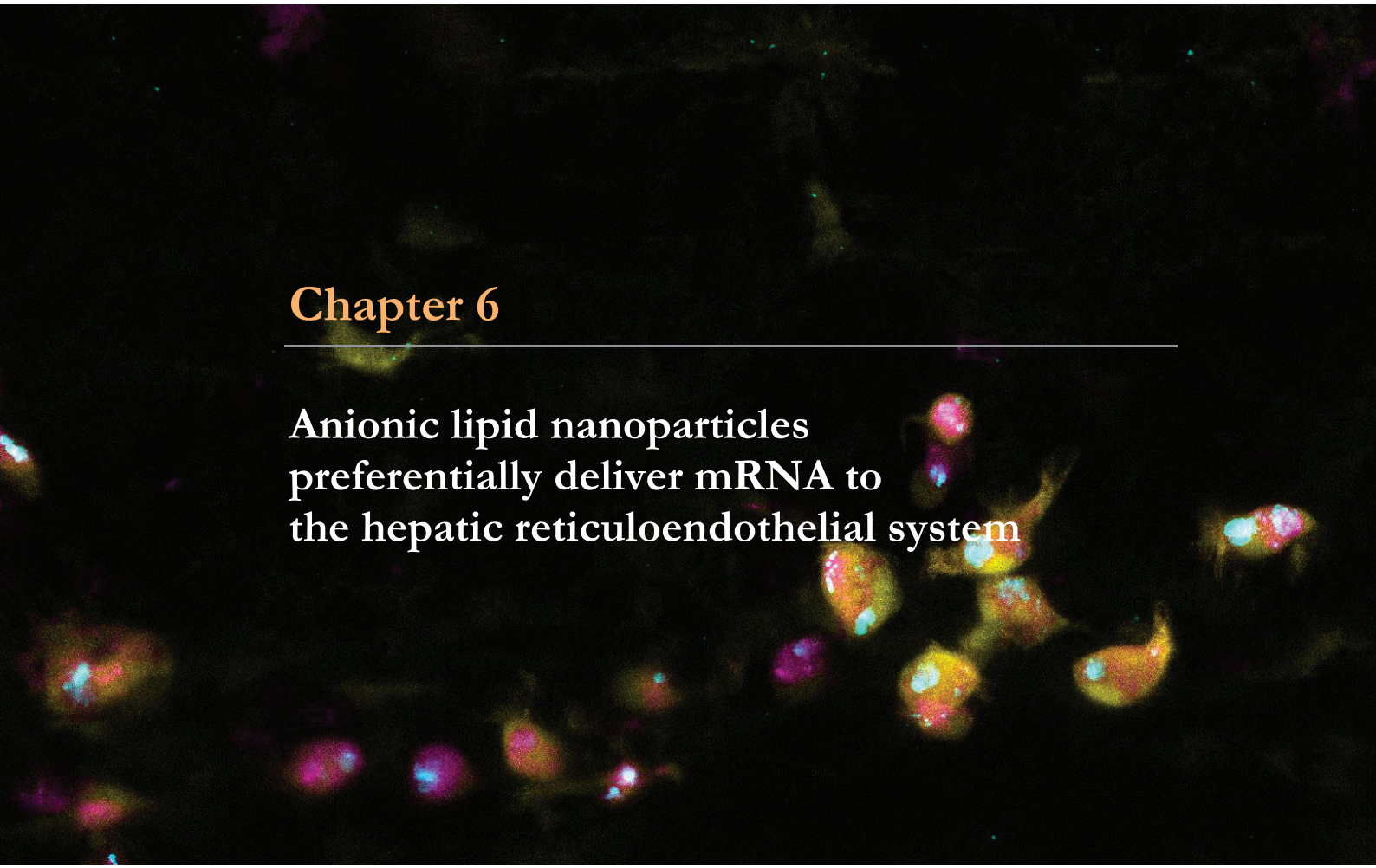

Chapter 6

Anionic lipid nanoparticles preferentially deliver mRNA to the hepatic reticuloendothelial system

Submitted:

Pattipeiluhu, R*; **Arias-Alpizar, G.***; Basha, G.; Bussmann, J.; Sharp, T.H.; Moradi, M.A.; Sommerdijk, N.; , J.; Cullis, P.R.; Kros, A.; Campbell, F. Anionic Lipid Nanoparticles Preferentially Deliver mRNA to the Hepatic Reticuloendothelial System. **Submitted.**

These authors contributed equally*

Image: Macrophages (in magenta) expressing GFP (in yellow) delivered by srLNP (in cyan) in a stabilin-1 & -2 double knockout zebrafish.

6.1 Abstract

Lipid nanoparticles (LNPs) are the leading non-viral technology for the delivery of exogenous RNA to target cells *in vivo*. These delivery platforms are exemplified by Onpattro®, a clinically approved LNP-based RNA interference (RNAi) therapy, indicated for polyneuropathies resulting from transthyretin-mediated amyloidosis, administered systemically, and targeted to parenchymal liver cells. The discovery of LNP technologies capable of preferential RNA delivery to liver cell types beyond hepatocytes has, however, proved more challenging. Here, preceded by a comprehensive mechanistic understanding of nanoparticle biodistribution and clearance, we design an LNP-based mRNA delivery platform capable of preferentially targeting the hepatic reticuloendothelial system (RES). Evaluated in embryonic zebrafish, validated in mice and compared to LNP-mRNA systems based on the lipid composition of Onpattro®, RES-targeted LNPs show significantly enhanced mRNA expression both globally within the liver and specifically within hepatic RES cell types. LNP redirection to the hepatic RES requires switching of LNP surface charge from neutral to anionic, achieved through just a single lipid change within the lipid composition of Onpattro®. Not only does this technology open up new opportunities to treat diseases in which RES cell types play a central role but it cements the view that rational development of advanced RNA therapies must be preceded by a thorough understanding of the nano-bio interactions involved.

6.2 Introduction

RNA therapy relies on cytosolic delivery of exogenous (therapeutic) RNA molecules, *e.g.* mRNA, siRNA, or miRNA, to gain precise control of gene expression within target cells.[1, 2] This requires delivery systems to protect, transport and deliver highly charged, immunogenic and membrane impermeable RNA payloads within target cells and tissues in the body. To this end, lipid nanoparticles (LNPs) have emerged as the state-of-the-art, non-viral RNA delivery system for *in vivo* application.[3-5] These technologies are exemplified by Onpattro®, a clinically approved LNP-based RNA interference (RNAi) therapy, administered intravenously (*i.v.*) and used to treat polyneuropathies resulting from transthyretin-mediated amyloidosis (hATTR).[6, 7] Onpattro® functions by transiently silencing (siRNA delivery) the expression of transthyretin (TTR) specifically within hepatocytes.[8] Hepatocyte targeting is mediated through the adsorption of soluble apolipoprotein E (apoE) to the surface of a circulating LNP.[8, 9] This, in turn, promotes LNP binding to the low density lipoprotein receptor (LDLr),[10] a receptor heavily expressed on the sinusoidal surface of hepatocytes. ApoE-LDLr binding leads to LNP endocytosis and consequent cytosolic siRNA delivery, which is enhanced by the protonation of ionizable (cationic) lipids within the endosome and subsequent disruption of the endosomal membrane.[11]

Following systemic administration, harnessing apoE-mediated LNP specificity for the delivery of RNA therapeutics (siRNA or mRNA) to hepatocytes is relatively common.[5, 10, 12-15] Expanding the scope of LNP-based gene therapies to other hepatic cell types (or non-hepatic cells), and therefore access a much greater diversity of disease states, however, has proved more challenging. To meet this challenge, high throughput empirical screening of DNA-barcoded LNPs has revealed formulations that preferentially target extra-hepatic tissues (*e.g.* bone marrow)[16] and cells (*e.g.* T-cells),[17] as well as individual hepatic (*e.g.* liver endothelial) cell types.[18, 19] However, while these empirical discoveries have undoubtedly enriched our understanding of the structure-activity landscape of LNP technologies, they have not revealed the biological mechanisms underpinning LNP transport and preferential cellular uptake *in vivo*. Only this knowledge enables the rational design of new LNP-based RNA therapies with target cell specificity.[5, 20]

Besides hepatocytes (comprising ~80% liver volume), the liver is composed of non-parenchymal liver cells, including Kupffer cells (KCs) and liver sinusoidal endothelial cells (LSECs).[21] Hepatic blood vessels, or sinusoids, connecting the

hepatic artery and portal vein to the central vein of the liver, are primarily composed of LSECs (~70%) and KCs (~20%).[22, 23] Together these two cell types make up the hepatic reticuloendothelial system (RES) whose primary role is to maintain blood homeostasis through the scavenging of macromolecular waste and pathogens from blood.[24, 25] LSECs, in particular, are specialized scavenger endothelial cells (SECs) and have one of the highest endocytic activities of any cell type in the body.[26] These cells are responsible for the clearance of endogenous macromolecules, such as oxidized low-density lipoprotein and hyaluronic acid,[25, 27, 28] as well as blood borne pathogens.[29, 30] In large part, LSEC clearance of macromolecular and pathogenic waste is mediated through an array of scavenger receptors (*e.g.* Hyaluronan- and Stabilin- receptors), heavily expressed on luminal membrane of LSECs.[31-33] As therapeutic target, LSECs not only play a crucial role in liver homeostasis, regeneration following acute injury, and in the pathogenesis of various liver diseases,[26, 34] but, as antigen presenting cells, are also key regulators of hepatic adaptive immunity and systemic immunotolerance.[35]

Guided by previous observations that *i.v.* administered anionic nanoparticles are extensively recognized and cleared by RES cell types,[36] here, we design anionic LNPs capable of preferentially targeting and transfecting the hepatic RES, *i.e.* scavenger receptor LNPs (srLNPs). This redirection required just a single lipid compositional change from the lipid formulation of Onpattro®. Evaluated within embryonic zebrafish *(Danio rerio),*[37] we qualitatively describe LNP biodistribution, mRNA delivery and expression of a fluorescent protein at cellular resolution, *in vivo* and in real time, with particular focus on relative LNP uptake and mRNA expression within SECs, macrophages and hepatocytes of the embryo. Furthermore, we confirm scavenger receptors, Stabilin-1 and -2, mediated uptake of anionic LNPs by SECs. Finally, we validate preferential LNP-mediated mRNA transfection of the hepatic RES in mice.

6.3 Results

Design and characterization of anionic srLNPs

Previously, we have shown that *i.v.* administered, anionic nanoparticles (ranging in size from 10-150 nm) are rapidly and extensively cleared from circulation by scavenging endothelial cells (SECs) within the posterior cardinal vein (PCV), caudal hematopoietic tissue (CHT) and caudal vein (CV) of a two day old zebrafish embryo. In teleost fish (*i.e.* zebrafish), and other aquatic vertebrates,

SECs are not located primarily in the liver, as for LSECs in mammals, but reside in various other organs including scavenging (venous) blood vessels.[38] Mechanistically, anionic nanoparticle recognition and uptake by SECs is mediated by the scavenger receptors, Stabilin-1 (*stab1*) and Stabilin-2 (*stab2*).[36] Stabilin-1 and Stabilin-2 are heavily expressed by LSECs in the mammalian liver[39] and *i.v.* injection of anionic liposomes in (young) adult mice results in extensive nanoparticle uptake within these cell types. In addition to SECs, anionic nanoparticles are also scavenged by blood resident macrophages, both within the CHT of the embryonic zebrafish and within the mouse liver (*i.e.* within KCs).[36, 40] All together, these observations indicate that the embryonic zebrafish can be used to qualitatively predict *in vivo* nanoparticle interactions with mammalian RES cell types.

Here, we aimed at rationally designing an anionic LNP system enabling genetic manipulation in hepatic RES cells. In general, LNPs consist of five structural components (four lipid reagents and an oligonucleotide payload) that self-assemble to form discrete nanostructures ranging from ~30 to ~150 nm in size (**Figure 1a**).[41] The "hydrophobic" core of an LNP is rich in ionizable lipids (*e.g.* DLin-MC3-DMA (50 mol%) *[in the case of Onpattro®]), cholesterol (38.5 mol%*) and an oligonucleotide payload. The LNP surface (*i.e.* lipid-water interface), in contrast, is rich in helper phospholipids (*e.g.* DSPC, 10 mol%*) and lipid-PEG conjugates (*e.g.* DMG-PEG2k, 1.5 mol%*).[42] We, therefore, hypothesized that switching the helper phospholipid of Onpattro®, from zwitterionic, 1,2-distearoyl-*sn*-glycero-3-phosphocholine (DSPC) to anionic, 1,2-distearoyl-*sn*-glycero-3-phosphoglycerol (DSPG), would render the LNP surface anionic. In turn, an anionic surface charge would redirect LNP targeting and functional RNA delivery from hepatocytes to the hepatic RES, by promoting Stabilin- mediated LNP recognition and uptake in LSECs whilst simultaneously inhibiting hepatocyte apoE-LDLr interactions (**Figure 1b,c**).[43] Hereafter, we refer to DSPG-containing LNPs as srLNPs and LNPs based on the lipid composition of Onpattro® as DSPC-LNPs (**Figure 1d**). In all cases, a nitrogen to phosphate (N/P) ratio of 6 was used, as is typical for larger nucleic acid payloads.[44]

Following microfluidic assembly, cryo-electron transmission microscopy (cryoTEM) revealed LNPs with a typical electron dense core structure (**Figure 1e**).[45-48] Within DSPC-LNPs (47.0 nm ± 13.9 nm), both amorphous and lamellar core structures were present, whereas the core structure of srLNPs (66.6 nm ± 22.0 nm) contained a mixture of amorphous, unilamellar and polymorphic

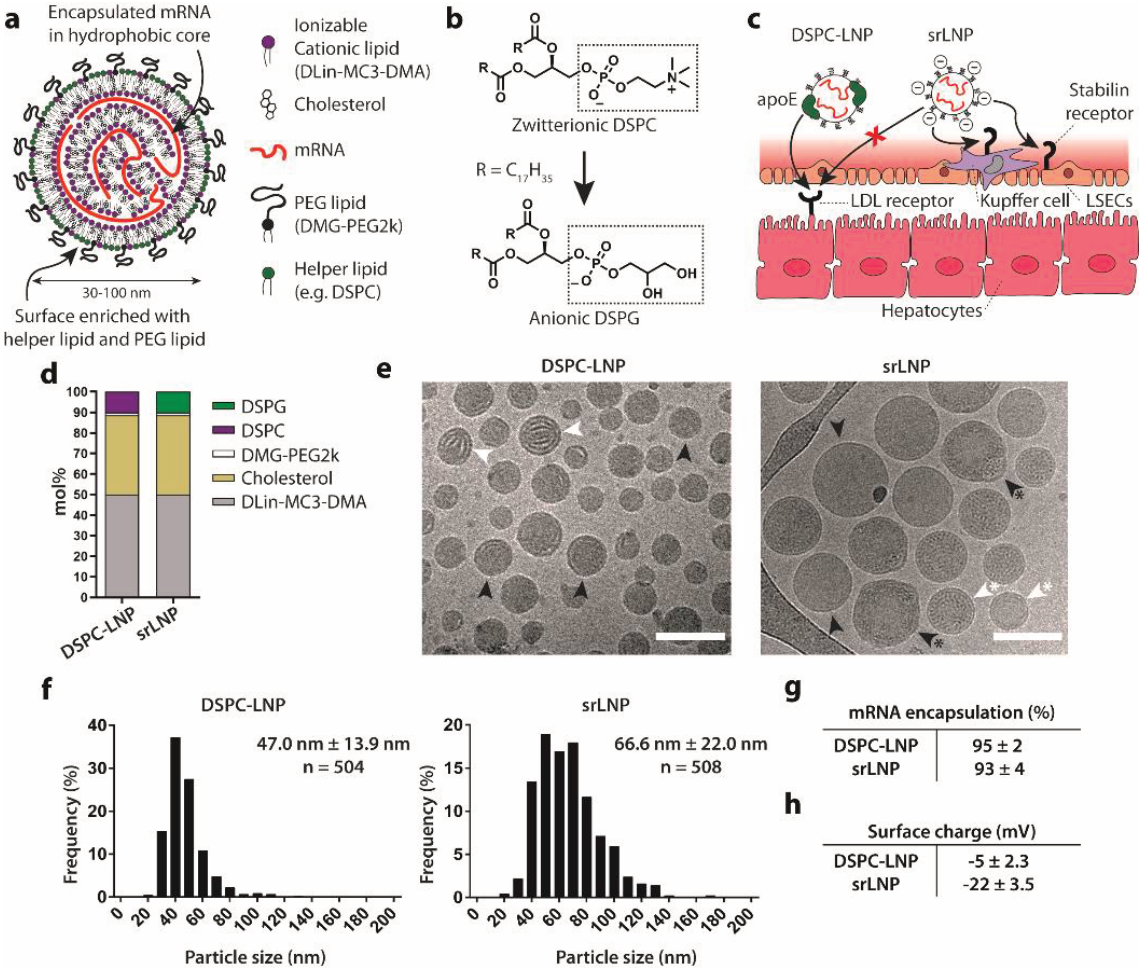

Figure 1 . Design and characterization of srLNPs. (a) Schematic of the structural organization of an LNP containing mRNA, as described previously.[42] Helper phospholipids (typically incorporated at 10 mol%) are enriched at the LNP surface. **(b,c)** Within the liver sinusoids, switching of the helper phospholipid from zwitterionic DSPC (as in Onpattro®) to anionic DSPG creates anionic srLNPs that are directed to the hepatic RES, *via* Stabilin receptor mediated recognition and uptake in LSECs. srLNP uptake within hepatic RES cells is further enhanced by the inhibition of apoE-LDLr interactions mediated by anionic phospholipids (*e.g.* DSPG).[43] The mechanism of recognition and uptake of srLNPs by blood resident macrophages (*i.e.* KCs) is not known. **(d)** Lipid composition of DSPC-LNPs (*i.e.* Onpattro®) and srLNPs. **(e)** CryoTEM images of DSPC-LNPs and srLNPs (entrapping capped mRNA-eGFP) show solid lipid nanoparticle structures. Scale bars: 100 nm. Internal structures indicated with arrows: lamellar (white), amorphous (black), polymorphous (black*) and unilamellar (white*) **(f)** Size distribution of DSPC-LNPs and srLNPs, as determined by cryoTEM. The values derived from the frequency distribution graphs represent the mean ± standard deviation. **(g)** mRNA encapsulation efficiency within DSPC-LNPs and srLNPs, as determined by RiboGreen assay. **(h)** Surface charge of DSPC-LNPs and srLNPs, as determined by zeta potential measurements. See **Supplementary Table 1** for full biophysical characterization of all formulations used in this study.

structures, as has been previously reported for LNP-mRNA systems.[49, 50] Particle sizes of both DSPC-LNPs and srLNPs (determined through cryoTEM image analysis) were comparable to the number-weighted average, as determined by dynamic light scattering (**Figure 1f** and **Supplementary Table 1**), and, in all cases, mRNA encapsulation efficiencies were >95% (**Figure 1g**). Importantly, however, srLNPs possessed a significantly more anionic (ζ-potential ~ -20 mV) surface charge compared to DSPC-LNPs (ζ-potential ~ -5 mV), indicative of DSPG exposed at the lipid-water interface (**Figure 1h**). For detailed biophysical characterization (*i.e.* size, surface charge, encapsulation efficiencies) of all formulations used in this study, please refer to **Supplementary Table 1**.

Biodistribution of LNPs in embryonic zebrafish

To assess LNP biodistribution, DSPC-LNPs and srLNPs, containing a fluorescent lipid probe (DOPE-LR, 0.2 mol%) and encapsulating fluorescent mRNA (capped and Cy5-labelled), were injected (*i.v.,* ~10 mM lipid, ~0.2 mg/kg mRNA) in wildtype zebrafish embryos at two days post-fertilisation (dpf) (**Figure 2a**). Confocal imaging of entire live embryos, as well as high resolution, tissue level views to include key scavenging cell types of the embryo within the CV and CHT (**Figure 2b**), revealed distinct biodistribution patterns for both LNP-mRNA formulations at 1.5 hour post injection (hpi) (**Figure 2c-f**). In the case of DSPC-LNPs, particles were mostly freely circulating, with both lipid and mRNA associated dyes confined to, and homogenously distributed throughout, the vasculature of the embryo (**Figure 2c,d**). In addition, a small fraction of DSPC-LNPs accumulated in blood-resident macrophages, within the CHT of the embryo, indicative of low level recognition and uptake by the RES (white arrowheads, **Figure 2d**; confirmed in *mpeg:*mCherry embryos**, Supplementary Figure 1a-c**). In the case of srLNPs, the majority of injected particles were cleared from circulation at 1.5 hpi, with highly selective accumulation observed within SECs and blood-resident macrophages within the PCV, CHT and CV of the two day old embryo (**Figure 2e,f**; macrophage uptake confirmed in *mpeg1:*mCherry embryos, **Supplementary Figure 1d-f**).

The selective accumulation of srLNPs within scavenging (venous) blood vessels of the embryonic zebrafish closely mirrored previously observed biodistributions of anionic liposomes, polymersomes and inorganic nanoparticles, in which nanoparticle uptake within SECs was mediated by the Stabilin scavenger receptors.[36] To confirm Stabilin-mediated uptake, srLNPs were injected (*i.v.*) in established *stab1*$^{-/-}$*/stab2*$^{-/-}$ double knockout (KO) zebrafish (2 dpf),[51] (described in **Chapter 3**). Within these mutant, srLNPs

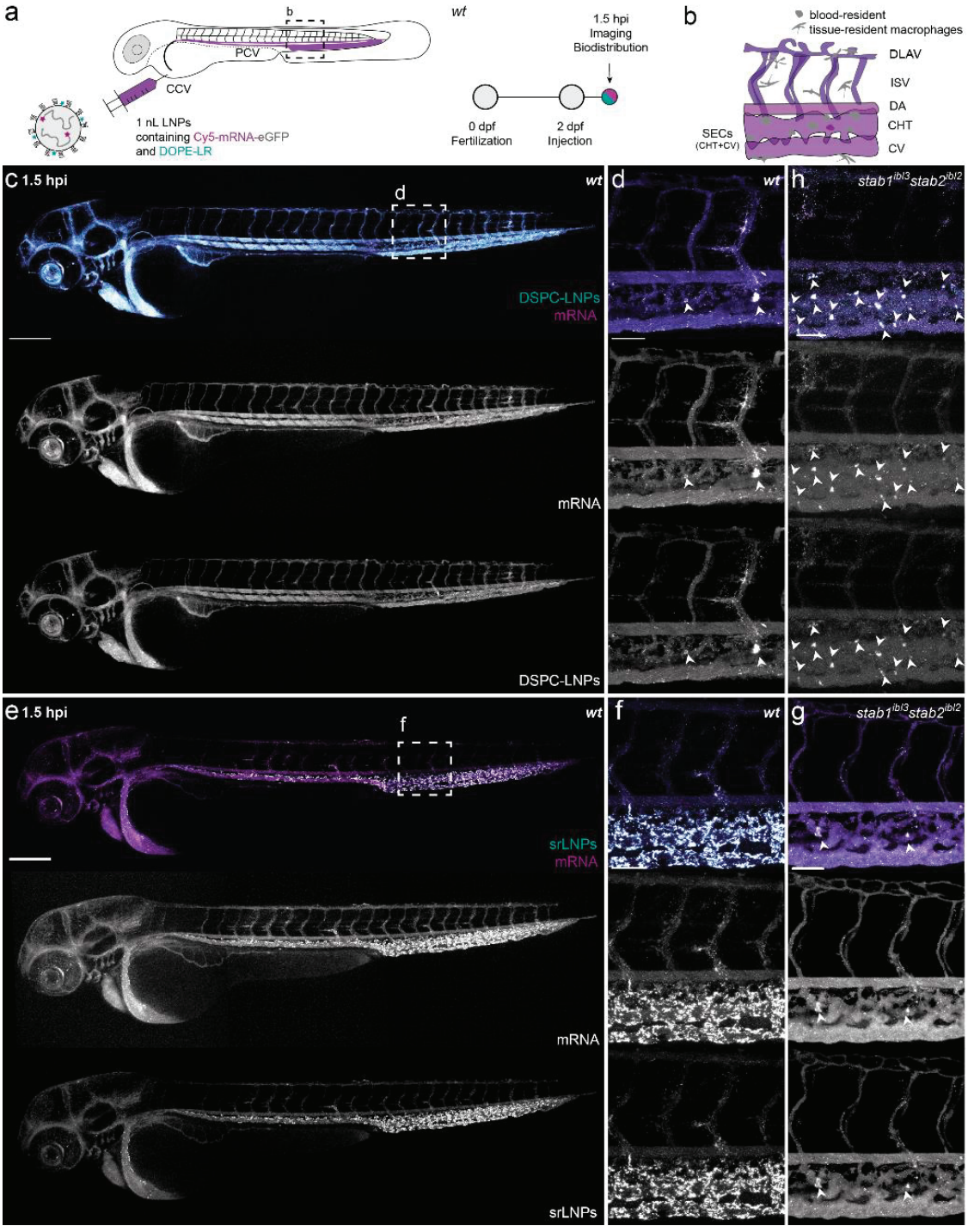

Figure 2. Biodistribution of DSPC-LNPs and srLNPs in two-day old embryonic zebrafish at 1.5 hpi. (a) Schematic showing the site of LNP injection (*i.v*) within embryonic zebrafish (2 dpf) and imaging timeframe. LNPs contained DOPE-LR (cyan, 0.2 mol%) as fluorescent lipid probe and Cy5-labelled eGFP mRNA (magenta) as fluorescent mRNA probe. Injected dose: ~10 mM lipid, ~0.2 mg/kg mRNA. Injection volume: 1 nl. Major venous blood vessels: CCV – common cardinal vein; PCV – posterior cardinal vein. **(b)** Tissue level schematic of a dorsal region of the embryo containing scavenging cell types (*i.e.* SECs and blood resident macrophages). Blood vessels: DA – dorsal aorta, CHT –

caudal hematopoietic tissue; CV – caudal vein; ISV – intersegmental vessel; DLAV - dorsal longitudinal anastomotic vessel**. (c,d)** Whole embryo (10x magnification) and tissue level (40x magnification) views of DSPC-LNP biodistribution within wildtype (*AB/TL)* embryonic zebrafish (2 dpf) at 1.5 hpi. DSPC-LNPs are mostly freely circulating, confined to, and distributed throughout, the vasculature of the embryo. Low level phagocytotic uptake within blood resident macrophages is highlighted by white arrowheads. **(e,f)** Whole embryo (10x magnification) and tissue level (40x magnification) views of srLNP biodistribution within wildtype embryonic zebrafish (2 dpf) at 1.5 hpi. srLNPs are mainly associated with SECs within the PCV, CHT and CV of the embryo and are largely removed from circulation at 1.5 hpi. Phagocytotic uptake of both DSPC-LNPs and srLNPs within blood resident macrophages at 1.5 hpi was confirmed by analogous LNP injections in Tg(*mpeg1*:mCherry) zebrafish embryos, stably expressing mCherry within macrophages (**Supplementary Figure 1**). **(g)** Tissue level (40x magnification) view of srLNP biodistribution within double knockout (*stab1*^{ibl3}*stab2*^{ibl2})[51] zebrafish embryos at 1.5 hpi. Within Stabilin KOs, srLNPs are now mostly freely circulating, with low level phagocytotic uptake within blood resident macrophages highlighted by white arrowheads**. (h)** Tissue level (40x magnification) view of DSPC-LNP biodistribution within double knockout (*stab1*^{ibl3}*stab2*^{ibl2})[51] zebrafish embryos at 1.5 hpi. Within *stabilin* KOs, DSPC-LNPs remain mostly freely circulating, with low level phagocytotic uptake within blood resident macrophages highlighted by white arrowheads. Scale bars: 200 μm (whole embryo) and 50 μm (tissue level).

predominantly remained in circulation at 1.5 hpi with a small fraction accumulating within blood-resident macrophages of the CHT (**Figure 1g** for the whole embryo and **Supplementary Figure 2**). This confirmed srLNPs selectively accumulate within RES cell types of the embryonic zebrafish and that recognition and uptake of srLNPs within SECs, but not macrophages, is mediated by Stabilin receptors. Analogous injections of DSPC-LNPs, within double KO embryos, did not alter DSPC-LNP biodistribution, with the majority of DSPC-LNPs remaining in circulation (**Supplementary Figure 1h** and **Supplementary Figure 2**). In all cases, both lipid and mRNA fluorescent probes, appear fully colocalized at 1.5 hpi, suggesting mRNA remains stably entrapped within the core of both DSPC- and srLNPs in circulation, as well as during (early) cellular recognition and uptake. Under the standard confocal microscope setups used in this study, it was not possible to resolve potential separation of lipid and mRNA fluorescent probes following endosomal rupture and cytosolic mRNA release.

LNP-mediated mRNA delivery and expression in embryonic zebrafish

To assess LNP-mediated delivery of functional mRNA within the embryonic zebrafish, it was first necessary to switch to unlabeled eGFP mRNA (capped, **Figure 3a**), as we consistently observed low mRNA expression levels using Cy5-labeled eGFP (capped) mRNA payloads. This alteration did not significantly

change the structure, surface charge or mRNA encapsulation efficiency of srLNPs (see **Supplementary Table 1**). At 1.5 hpi, srLNPs (~10 mM lipid, ~0.2 mg/kg mRNA) again associated with SECs and blood-resident macrophages within the PCV, CHT and CV of the embryonic zebrafish (**Figure 3b,c**). Given the intrinsic timeframe for mRNA delivery, expression and maturation of eGFP,[52, 53] low level green fluorescence observed at 1.5 hpi, within the yolk sac and iridophores (pigment cells) of the embryo, can be attributed to embryo autofluorescence in the GFP channel.[54] At 24 hpi, however, intense eGFP fluorescence was observed specifically within SECs and blood-resident macrophages of the embryo (**Figure 3d,e**). This timeframe is consistent with reported eGFP-mRNA delivery and expression timeframes using analogous lipid-based delivery systems,[52] whereby the onset of eGFP maturation and fluorescence (*in vitro)* occurs 2-7 h post-incubation and expression levels (fluorescence intensity) continually increase up to 24 h post-treatment.[55] Within *stab1*$^{-/-}$*/stab2*$^{-/-}$ KO embryos, srLNP-mediated eGFP expression, at 24 hpi, was observed only within blood-resident macrophages and not SECs, confirming macrophage uptake of srLNPs, as for other anionic nanoparticles, is not dependent on Stabilin receptors (**Supplementary Figure 3**).

For srLNPs, the exogenous eGFP expression pattern mirrored srLNP biodistribution at 1.5 hpi (**Figure 2e,f**), confirming successful transport, uptake and cytosolic delivery of functional mRNA within these cells. This is particularly remarkable given SECs have one of the highest endo/lysosomal activities of any cell type in the body,[28, 33] and are therefore primed to breakdown fragile RNA molecules. Endosomal escape and cytosolic delivery of RNA is widely recognized as one of the major obstacles in the development of effective RNA therapies,[56] with <2% of internalized siRNA (complexed within LNPs based on the lipid composition of Onpattro®) reaching the cytoplasm of HeLa cells *(in vitro)* and hepatocytes *(in vivo)*.[57, 58] Indeed, the acute extent of mRNA degradation within SECs (as well as potential mRNA degradation in circulation), was, in part, confirmed by injection (*i.v.*) of free eGFP-mRNA (capped; both cy5-labeled and unlabeled) within the zebrafish embryo. This resulted in no significant expression of eGFP within SECs at 24 hpi despite extensive accumulation within these cells at 1.5 hpi (presumably *via* scavenger receptor-mediated uptake of circulating, polyanionic RNA)[59] (**Supplementary Figure 4**).

In the case of DSPC-LNP (~10 mM lipid, ~0.2 mg/kg mRNA) mediated mRNA delivery, widespread eGFP fluorescence was observed throughout the wildtype embryo at 24 hpi (**Supplementary Figure 5**). Combined with the evident lack of cellular accumulation at 1.5 hpi (**Figure 2c,d**), this indicates low-level, non-

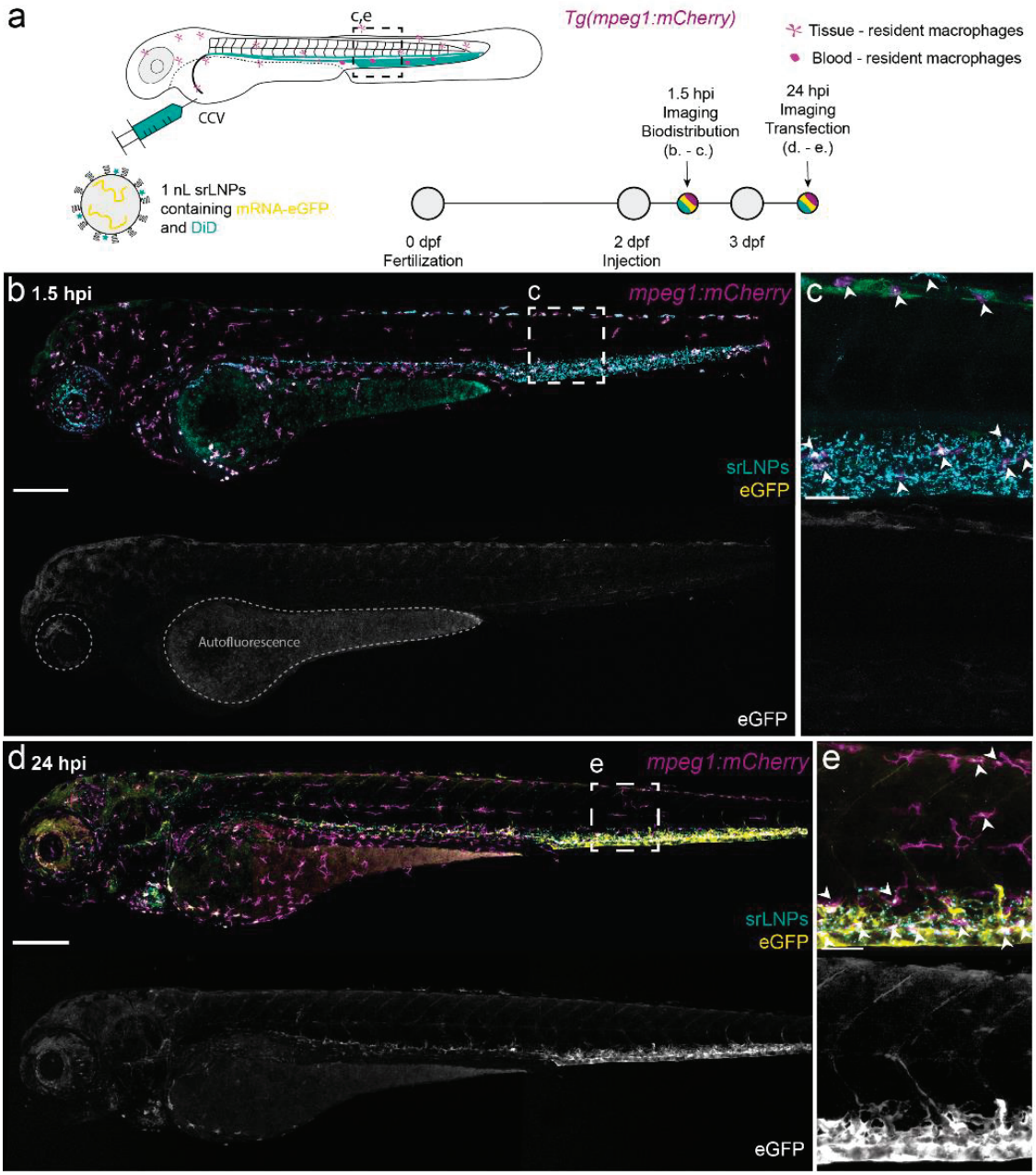

Figure 3. srLNP biodistribution, eGFP-mRNA delivery and eGFP expression within *mpeg1:*mCherry transgenic zebrafish embryos at 1.5 and 24 hpi. (a) Schematic showing the site of srLNP injection (*i.v.*) within embryonic zebrafish (2 dpf) and imaging timeframe. srLNPs contained DiD (cy5, 0.1 mol%) as fluorescent lipid probe and unlabeled, eGFP mRNA (capped) payload. Injected dose: ~10 mM lipid, ~0.2 mg/kg mRNA. Injection volume: 1 nl. Tg*(mpeg1*:mCherry*)* zebrafish embryos stably express mCherry (magenta) within all macrophages**. (b,c)** Whole embryo (10x magnification) and tissue level (40x magnification) views of srLNP biodistribution and eGFP expression within the embryonic zebrafish at 1.5 hpi. srLNPs were associated with SECs and blood resident macrophages (white arrowheads) within the PCV, CHT and CV of the embryo. Low level autofluorescence in the GFP channel is highlighted within the yolk sac and pigment cells of the embryo. **(d,e)** Whole embryo and tissue level views of srLNP

biodistribution and eGFP expression within the embryonic zebrafish at 24 hpi. At this timepoint, srLNPs remain associated with SECs and blood resident macrophages (white arrowheads) within the PCV, CHT and CV of the embryo. However, intense eGFP expression was now observed specifically within the PCV, CHT and CV confirming successful cytosolic delivery and translation of functional eGFP mRNA within SECs and blood resident macrophages. Scale bars: 200 μm (whole embryo) and 50 μm (tissue level).

specific cellular uptake of LNPs, based on the lipid composition of Onpattro®, with concurrent mRNA expression across a broad range of cell types, including SECs and blood-resident macrophages. Importantly, however, at 2 dpf, the liver of the embryonic zebrafish has yet to develop.[60, 61] To assess *in vivo* LNP interactions with a functional liver system, and potentially corroborate reported hepatocyte targeting of Onpattro® in adult mammals, it was therefore necessary to switch to LNP injections in older zebrafish embryos.

Hepatocyte targeting and mRNA expression in older zebrafish embryos

From approximately 55 hours post-fertilisation (hpf), the liver of the embryonic zebrafish undergoes a dramatic growth phase. New intrahepatic blood vessels are formed, with blood circulation detected from 72 hpf,[62] and the localised expression of key hepatocyte markers, including transferrin (Tf)[63] and liver fatty acid binding protein (L-FABP),[64] evidently marking maturation of functional hepatoctyes. During this growth phase, anatomical features, characteristic of the mammalian liver, and important for the correct processing of lipid nanoparticles, also emerge, including a Space of Disse,[65] the likely presence of a fenestrated endothelium,[66] and a functional biliary network (connected to the blood vasculature *via* hepatocytes).[60] These features, combined with a conserved repertoire of lipid transport proteins,[67, 68] including apoE, and lipoprotein receptors, including LDLR,[69, 70] suggest older (> 72 hpf) zebrafish embryos may offer an attractive *in vivo* model to assess endogenous lipid transport mechanisms, including lipid processing disorders,[71] and mechanistically probe their prospective role in the fate of LNPs in higher order mammalian systems.

To verify liver developmental timeframes, and to assess the suitability of the embryonic zebrafish as a predictive *in vivo* model for hepatocyte targeting of nanomedicines, non-PEGylated liposomes (~100 nm), co-formulated with cholesterol-conjugated, human apoE target peptides (Chol-NH-apoE peptide, 5 mol%,), were administered within 3 and 4 day old zebrafish embryos (*L-FABP:*eGFP transgenic line, stably expressing L-FABP-eGFP fusion proteins within hepatocytes) (**Figure 4a,b**).

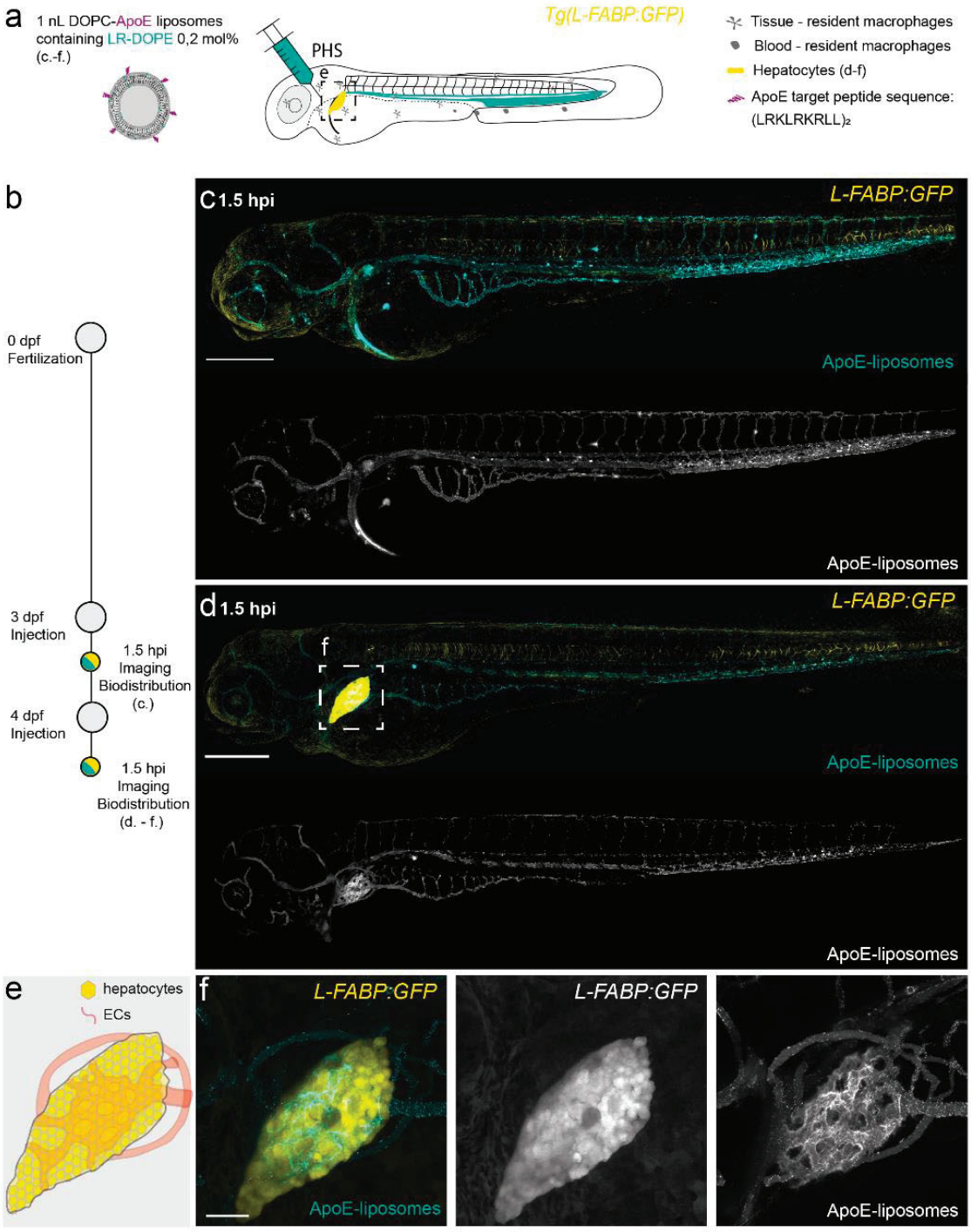

Figure 4. Biodistribution of apoE-targeted liposomes in three- and four-day old zebrafish embryos. (a) Schematic showing the site of apoE-targeted liposome injection (*i.v.*) within embryonic zebrafish (at 3 and 4 dpf). Liposomes contained 0.2 mol% DOPE-LR as fluorescent lipid probe (cyan). Injected dose: ~5 mM lipid, ~5 mol% ApoE target ligand (amino acid primary sequence: $(LRKLRKRLL)_2$), Injection volume: 1 nl. Tg(*L-FABP:*eGFP) zebrafish embryos stably express eGFP (yellow) within hepatocytes. PHS – primary head sinus. **(b)** Injection and imaging timeframe**. (c,d)** Whole embryo (10x magnification) views of apoE-targeted liposome biodistribution within **(c)** three- and **(d)**

four-day old embryonic zebrafish at 1.5 hpi. **(e)** Tissue level schematic of the embryonic liver at 4 dpf**. (f)** Tissue level (40x magnification) views of apoE-targeted liposome biodistribution within the liver of a four-day old embryo. Within the embryonic liver, liposomes appear predominantly associated with ECs and not hepatocytes. Scale bars: 200 μm (whole embryo) and 50 μm (tissue level).

Nanoparticle/macromolecule-conjugated, human apoE target peptides (*amino acid sequence*: $(LRKLRKRLL)_2$; tandem-repeat LDLR target sequence (residues 159-167) of human apoE) have been previously shown to interact with LDLr, as well as the low-density lipoprotein receptor-related proteins, LRP1 and LRP2.[72-74] Following liposome (~5 mM) administration within a zebrafish embryo (3 dpf), no significant fluorescence (eGFP) was observed in the region of the developing liver and apoE-targeted liposomes were mostly freely circulating (**Figure 4c**). At 4 dpf, however, the liver of the embryo, delineated by transgenic eGFP-*L-FABP* fluorescence, became evidently present and *i.v.* administered apoE-targeted liposomes now clearly accumulated within the liver vasculature (**Figure 4d-f**). Interestingly, at 1.5 hpi, we observed no significant colocalization of apoE-targeted liposomes and hepatocytes within the liver. This may be due to liposome stockpiling within the Space of Disse, as has also been described for the hepatic clearance of albumin within embryonic zebrafish (12 dpf).[66] Crucially, however, unmodified DOPC liposomes did not accumulate within the embryonic liver of either a three- or four-day old embryo, confirming liver accumulation of apoE-targeted liposomes within a four-day old zebrafish embryo is exclusively mediated by apoE target peptides (**Supplementary Figure 6**). Overall, these observations corroborate the reported timeframe for both hepatic development and hepatocyte maturation within the zebrafish embryo and confirm apoE-mediated targeting of nanoparticles to the liver of the zebrafish embryo is possible from 4 dpf.

Having verified apoE-mediated liver targeting of liposomes, we next injected DSPC-LNPs (~10 mM, ~0.2 mg/kg mRNA, Figure 5a-e; ~30 mM, ~0.6 mg/kg mRNA, **Figure 5f-i**) and srLNPs (~30 mM, ~0.6 mg/kg mRNA, **Supplementary Figure 7**) in four day old zebrafish embryos. In the case of srLNPs, particles remained largely associated within the PCV, CV and CHT of the 4 day old embryo at 1.5 hpi, and exogenous eGFP expression was primarily restricted within ECs of these venous blood vessels at 24 hpi. No significant srLNP accumulation (at 1.5 hpi) or mRNA expression (at 24 hpi) was observed within the liver, confirming RES targeting of srLNPs remains predominant even in the presence of a functional liver system and functional hepatocytes. In the case of DSPC-LNPs (~10 mM), no significant LNP liver accumulation (1.5 hpi) nor liver specific eGFP

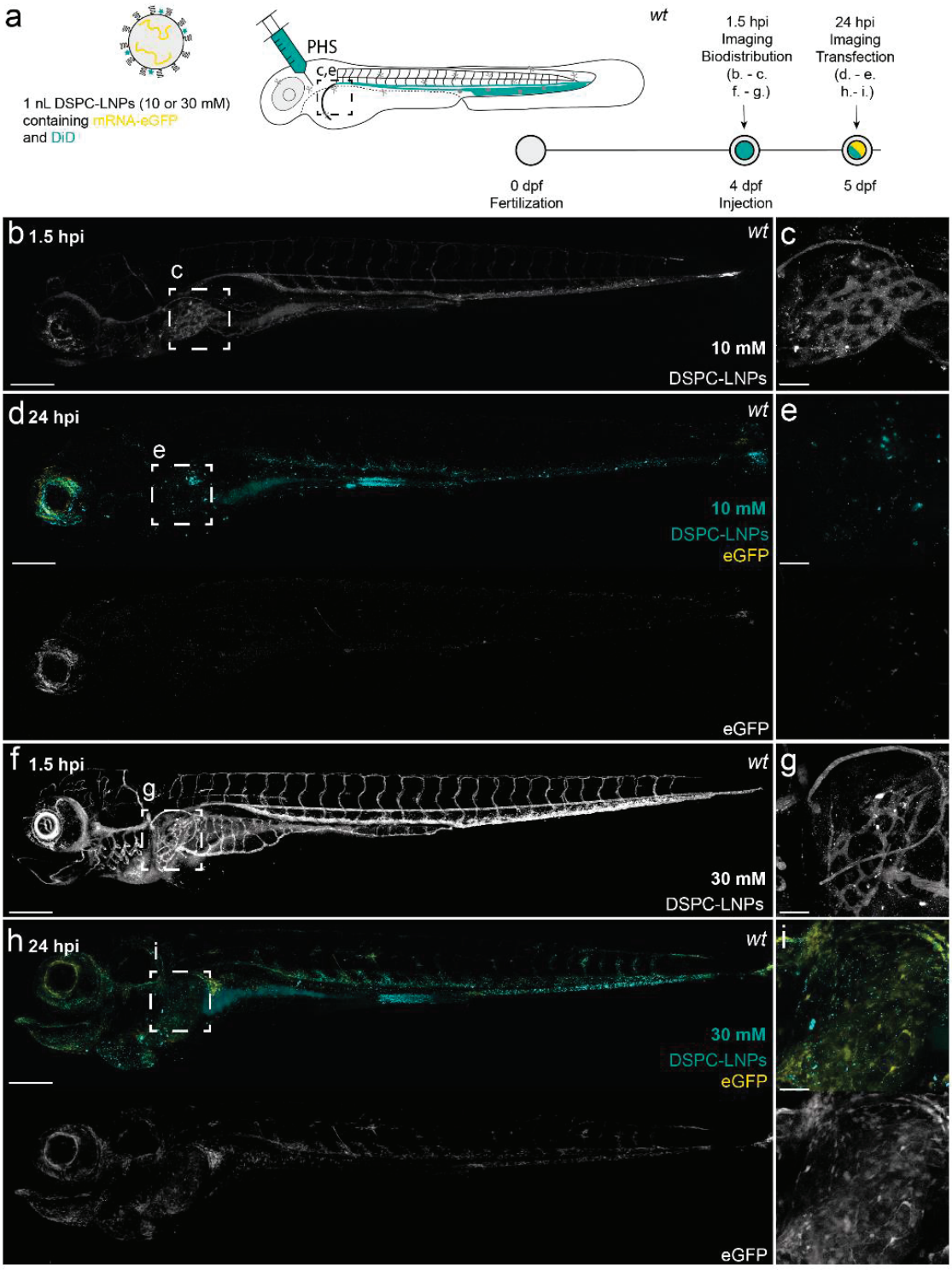

Figure 5. DSPC-LNP (10 and 30 mM) biodistribution and mRNA expression within, four-day old, wildtype (AB/TL) embryonic zebrafish. (a) Schematic showing the site of DSPC-LNP injection (*i.v.*) within embryonic zebrafish (4 dpf). DSPC-LNPs contained DiD (0.1 mol%) as fluorescent lipid probe and unlabeled, eGFP mRNA (capped) payload. Injection and imaging timeframe. Injection volume: 1 nL. PHS – primary head sinus. **(b,c)** Whole embryo (10x magnification) and tissue level (liver region, 40x magnification) views of DSPC-LNP biodistribution at 1.5 hpi. Injected dose: ~10 mM lipid, ~0.2 mg/kg

mRNA. LNPs were mostly freely circulating with no significant accumulation in the liver at 1.5 hpi. Intense fluorescent punctae within the liver region are likely due to macrophage uptake. **(d,e)** Whole embryo (10x magnification) and tissue level (liver region, 40x magnification) views of eGFP expression at 24 hpi. **(f,g)** Whole embryo (10x magnification) and tissue level (liver region, 40x magnification) views of DSPC-LNP biodistribution at 1.5 hpi. Injected dose: ~30 mM lipid, ~0.6 mg/kg mRNA. At both dosages, LNPs were mostly freely circulating with no significant accumulation in the liver observed at 1.5 hpi. Intense fluorescent punctae within the liver region are likely due to macrophage LNP uptake. **(h,i)** Whole embryo (10x magnification) and tissue level (liver region, 40x magnification) views of eGFP expression at 24 hpi. At 30 mM dosage, low level eGFP fluorescence is observed throughout the embryo, including within the liver region. Confocal microscope settings were identical across all experiments. Scale bars: 200 μm (whole embryo) and 50 μm (tissue level).

expression (24 hpi) was observed within the four day old embryo (**Figure 5b-e**). Increasing the dose threefold (~30 mM), however, did result in significant eGFP expression throughout the entire embryo, including the region of the liver (**Figure 5f-i**). Again, with no apparent targeting of DSPC-LNPs within the liver at 1.5 hpi, these observations indicate that DSPC-LNPs ineffectively target functional hepatocytes of the embryonic zebrafish *via* endogenous apoE-mediated lipid trafficking pathways and are instead liable to low-level non-specific uptake, with concurrent mRNA delivery and expression across a wide range of cell types.

LNP-mediated mRNA delivery and expression in mice

Having demonstrated RES specific mRNA transfection in embryonic zebrafish, we finally validated LNP biodistribution and LNP-mediated mRNA expression patterns in (young) adult mice. In particular, we focused on cell-specific LNP distribution and mRNA expression within the murine liver, the largest RES organ in mammals. For all mice experiments, LNP-mRNA formulations were injected (*i.v.*) in C57BL/6 mice (**Figure 6a**). To assess LNP distribution and functional mRNA delivery within individual hepatic and non-hepatic (*i.e.* spleen) RES cell types following *i.v.* administration, mice were anesthetized, a trans-cardiac collagenase perfusion performed, (parenchymal and non-parenchymal hepatic) cells separated, and individual cell types detected using cell-specific antibodies (**Supplementary Figure 8** for representative flow cytometry density plots). To monitor LNP biodistribution across RES cell types and tissues, LNP-mRNA formulations, containing a non-exchangeable, fluorescent lipid probe (DiD, 0.5 mol%), were administered (**Figure 6b**). At 2 hpi, for both DSPC- and srLNPs (42.75 mg/kg total lipid), we observed striking LNP accumulation within mouse liver cell types (**Figure 6c**) compared to those of the spleen (**Supplementary**

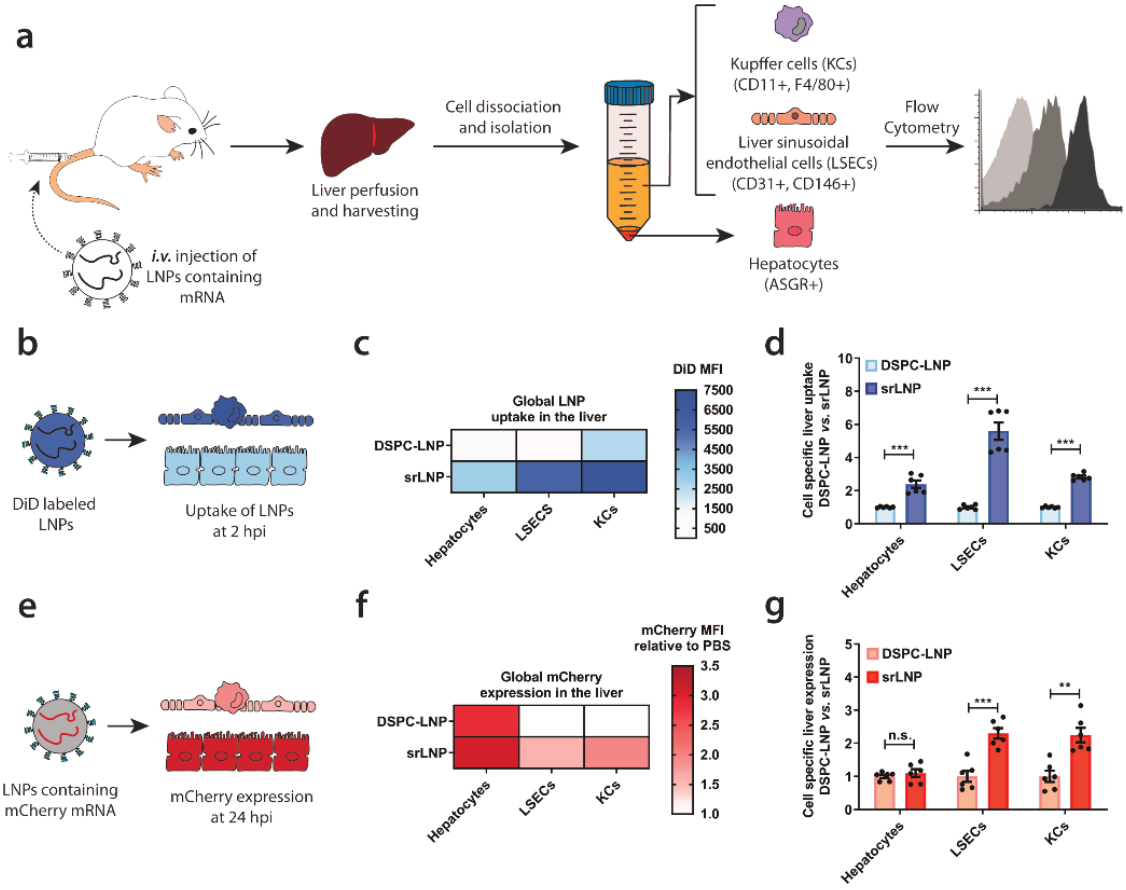

Figure 6. LNP uptake and functional mRNA delivery within different hepatic cell types. (a) Schematic illustrating the procedure to isolate different hepatic cell types and determine LNP-mRNA targeting and functional mRNA delivery. Following intravenous LNP-mRNA injection (*i.v.*) the liver was perfused with collagenase IV, hepatic cells were isolated and stained with specific antibodies, and flow cytometry was used to analyze LNP uptake and gene expression. Specific antibody markers used to uniquely identify hepatocytes, LSECs and KCs, respectively, are defined in parentheses. **(b)** For intrahepatic biodistribution studies, LNPs contained DiD (0.5 mol%) as fluorescent lipid probe. Cellular uptake of DSPC-LNP and srLNP was assessed following mouse sacrifice at 2 hpi. Injected dose: 42.75 mg/kg total lipid. **(c)** Heatmap of global LNP uptake in the liver determined by absolute DiD fluorescence. srLNP demonstrate significantly enhanced LNP uptake within all hepatic cell types, and significant re-direction to hepatic RES compared to DSPC-LNPs**. (d)** Cell specific liver uptake normalized to DSPC-LNP for each cell type**. (e)** For gene expression experiments, LNPs contained capped, mCherry-mRNA. Functional mRNA delivery was assessed based on mCherry fluorescence levels following mouse sacrifice at 24 hpi**. (f)** Heatmap of mCherry expression in different liver cell types following functional mRNA delivery using DSPC-LNP and srLNP. Injected dose: 0.25 mg/kg mRNA. **(g)** Cell specific mCherry expression normalized to DSPC-LNP for each cell type. In all cases, n=6 represents 3 separate liver tissue samples from 2 mice sorted into individual cell types. Bars and error bars in **d** and **g** represent mean ± s.e.m. The data was normalized to the average uptake and expression of DSPC-LNPs within each cell type. Statistical significance was evaluated using a two-tailed unpaired Student's t-test. n.s.= not significant, ** $p < 0.01$, *** $p < 0.001$. Exact P values for **d**: Hepatocytes P= 0.00011, LSECs P= $1.12*10^{-5}$, KCs P= $3.62*10^{-9}$. Exact P values for **g**: Hepatocytes P= 0.464, LSECs P= 0.00064, KCs P= 0.0023.

Figure 9), which although smaller than the liver is a highly efficient unit of the mononuclear phagocyte system.[75] Notably, both LNP formulations distributed to all individually isolated cell types within the liver, as has previously been described for LNP formulations based on Onpattro®.[76, 77] However, srLNPs demonstrated significantly enhanced uptake ($P < 0.001$) within all liver cell types relative to DSPC-LNPs (**Figure 6d**). This confirmed that incorporating anionic DSPG into LNP-mRNA delivery systems not only enhances liver tropism in general but also leads to a significant shift towards LNP targeting and cellular uptake within hepatic RES cell types.

To confirm functional mRNA delivery to hepatic RES cells, LNPs entrapping capped mCherry-mRNA (0.25 mg/kg mRNA) were administered in C57BL/6 mice (**Figure 6e**). This dosage is in line with other systemically administered LNP-mRNA therapies, including those currently in clinical trials (*e.g.* NCT03829384).[78] Following organ isolation and cell separation at 24 hpi, both srLNPs and DSPC-LNPs yielded comparable mCherry protein expression in hepatocytes, as well as within splenic RES cell types (**Figure 6f** and **Supplementary Figure 9**). In contrast, srLNPs yielded significantly enhanced functional mRNA delivery to hepatic RES cell types relative to DSPC-LNPs ($P < 0.001$) (**Figure 6g**). Importantly, for both srLNPs and DSPC-LNPs, absolute mCherry expression levels within hepatocytes were significantly higher than any other cell type analyzed. This apparent disparity between LNP cellular targeting and functional mRNA expression is likely explained, at least in part, by the adverse (high) endosomal activity within LSECs and KCs (leading to significant mRNA degradation despite extensive LNP internalization), combined with the extremely high translational proficiency of hepatocytes (leading to significant mRNA expression despite comparably low LNP internalization).[79] Interestingly, a four-fold dosage increase (1 mg/kg mRNA) resulted in significantly enhanced absolute mRNA expression within LSECs relative to hepatocytes and KCs, indicative perhaps of dynamic competition between these cell types in recognizing and internalizing LNPs (**Supplementary Figure 10**). Given no LNP technology has yet demonstrated exclusive targeting to a single cell type *in vivo*, these findings reaffirm the importance of considering not only LNP biodistribution but also cellular physiology (both in the healthy and diseased state) in the development of new LNP technologies with novel targeting function.

Overall, our data confirm that charge modifications to an LNP surface leads to preferential targeting of the hepatic RES and a significant increase in the absolute levels of functional mRNA expression within these cell types.

6.4 Discussion and Conclusion

Founded on prior knowledge of the fundamental mechanisms of anionic nanoparticle clearance *in vivo*,[36] (**Chapter 1 & 2**) we develop an LNP platform capable of preferentially targeting the hepatic RES, leading to enhanced mRNA expression within hepatic RES cell types. Given the importance of the hepatic RES in establishing and maintaining the liver microenvironment, as well as the pathogenesis of many liver,[26, 80] blood and (auto)immune diseases,[35] it is our belief that anionic LNP formulations should form the basis of future RNA gene therapies, against acquired and inherited diseases in which hepatic RES cell types play a central role.[34] Here, it is also important to recognize the extensive refinement of both ionizable[81-83] and sterol lipid components of LNPs[50] (primarily to promote endosomal rupture/escape and cytosolic RNA delivery), as well as chemical modifications to RNA (to improve stability, translation proficiency and reduce immunogenicity), that have already been made.[84-86] Incorporated within LNPs, these reagents can improve transfection efficiency >10-fold, compared to LNP systems based on the lipid composition of Onpattro®.[81, 82] These reagents are fully transferable to anionic, srLNP formulations and, if necessary, could be retrofitted to widen any potential therapeutic window.

Existing LNP technologies that have demonstrated preferential RNA delivery to non-parenchymal hepatic cell types and/or non-hepatic cells. Importantly, these technologies have all been discovered through bottom-up empirical screens and have not revealed the biological mechanisms underpinning any observed cellular preference. Preferential delivery of mRNA to liver ECs has, for example, been achieved through replacement of cholesterol with either cholesteryl oleate or oxidized cholesterol components.[18, 19] While these observations may conform to a charge-dependent, Stabilin-mediated mechanism of uptake within LSECs, as has been observed for both OxLDL and AcLDL,[27, 87] in the absence of reported zeta potentials and given both sterol reagents likely predominate within the LNP core, this may equally point to an alternative, viable mechanism of LNP recognition and uptake within hepatic RES cell types. Alternatively, exclusive LNP-mediated RNA delivery to the spleen has been achieved through the addition of the anionic phospholipid, 18PA (up to 30 mol%), added to the lipid composition of Onpattro®.[88]

Assuming the measured surface charge of these formulations is also anionic (and given srLNPs showed negligible accumulation within the spleen), this suggests

simply rendering an LNP anionic does not necessarily guarantee preferential uptake within hepatic RES cell types. Overall, these studies highlight the complex interplay between LNP compositional makeup, biophysical properties and structure, and the implications these factors have in determining the fate of an LNP *in vivo*. Given the vast exploitable chemical space of an LNP, the targeting of innate immune cells and hepatocytes – primed to recognize and internalize waste and/or pathogenic (lipid) particles – may therefore reflect the low-hanging fruit of preferential LNP tropisms. Therefore, the discovery of new LNP platforms capable of preferential targeting beyond RES cells and/or hepatocytes will likely benefit from a more focused and informed screening approach.

To this end, the elucidation and exploitation of the fundamental mechanisms dictating both endogenous and exogenous lipid particle fate *in vivo* can focus and direct empirical screens for novel LNP formulations. It is worth emphasizing that all cells rely, to some extent, on systemic lipid transport to ensure correct function. In light of this, we believe the embryonic zebrafish is a powerful addition to the discovery pipeline for new LNP technologies, both as a screening platform and as a tool to probe fundamental biology. As a screening and optimization tool, zebrafish embryos permit real-time, *in vivo* visualization of total LNP injected doses at cellular resolution. Furthermore, with a conserved repertoire of RES cell types, hepatocytes, soluble lipid transport proteins and receptors, the data acquired within these animals can offer qualitative predictions of cell specific LNP recognition and uptake within key mammalian RES organs. Furthermore, up to 5 dpf, the number of different LNP formulations that can be screened is limited only by practical considerations of time and capacity. As a fundamental tool to elucidate biological mechanisms underpinning LNP transport and RNA delivery, the short generational time of the zebrafish (approx. 3 months), the extensive repertoire of established (fluorescent) transgenic lines and antibodies,[89, 90] optimized techniques for genetic manipulation (including CRISPR/Cas9)[91] and advanced imaging techniques, enable key nano-bio interactions underpinning LNP fate *in vivo* to be comprehensively assessed and rapidly confirmed.

In conclusion, the widespread evaluation of LNP-based mRNA therapies as potential prophylactic vaccines,[92, 93] most notably against COVID-19,[94-97] has provided further proof of the broad therapeutic potential of these platform mRNA technologies. However, despite the obvious differences in therapeutic target, mode of action and injection site, all LNP-mRNA vaccine candidates closely resemble the lipid composition of Onpattro®. In particular, LNP surface lipids (*i.e.* "helper" phospholipids and PEG lipids), cholesterol content and overall

lipid composition are strikingly similar between different clinical formulations. Based on our observations, these vaccine candidates can be expected to elicit broad mRNA expression profiles. Indeed, following intramuscular (*i.m.)* injection of an LNP-mRNA COVID-19 vaccine candidate, mRNA (coding for the receptor binding domain (RBD) of SARS-CoV-2) expression was observed across a broad spectrum of cell types, including intramuscular and hepatic immune cells, as well as hepatocytes.[94] However, while the ability to leverage a wide array of cell types to produce a therapeutic protein may be safe and effective as a systemic secreted therapy (*i.e.* suitable for vaccine applications), the lack of LNP designs capable of preferentially delivering RNA to specific diseased cells and tissues in the body remains a major limitation. Although cell specificity, and therefore therapeutic windows, of LNP-mRNA systems can be enhanced, for example, through microRNA regulation of mRNA expression,[98] these technologies still rely on LNPs reaching and delivering functional mRNA within target cells at therapeutically relevant doses. To this end, we believe a top-down approach to LNP discovery, based on pre-existing knowledge of the nano-bio interactions, can guide and focus (high throughput) empirical screening. This will expedite the discovery of new LNP designs with inherent tropisms for specific and varied cell types.

6.5 Materials and Methods

Materials and Reagents

Dimethylformamide (DMF), piperidine, acetic anhydride, pyridine, trifluoroacetic acid (TFA) and acetonitrile (MeCN) were purchased from Biosolve (Valkenswaard, The Netherlands). N,N-diisopropylethylamine (DIPEA), and Oxyma were obtained from Carl Roth GmbH & Co (The Netherlands). Dichloromethane (DCM) and diethyl ether were supplied by Honeywell (Amsterdam, The Netherlands). Fmoc-Rink Amide AM resin was obtained from IRIS Biotech GmbH (Marktredwitz, Germany). All amino acids were supplied by NovaBioChem, (Zwijndrecht, The Netherlands), a subsidiary of Merck. 1,2-distearoyl-*sn*-glycerol-3-phosphocholine (DSPC), 1,2-distearoyl-*sn*-glycero-3-phospho-(1'-rac-glycerol) (DSPG), 1,2-dioleyl-*sn*-glycerol-3-phosphocholine (DOPC) and 1,2-dimyristoyl-rac-glycero-3-methoxypolyethylene glycol-2000 (DMG-PEG2k) were purchased from Avanti Polar Lipids (Alabaster, AL, US) or Lipoid GmbH (Ludwigshafen, Germany). All other chemicals were purchased from Merck (Zwijndrecht, The Netherlands). (6Z,9Z,28Z,31Z)-heptatriaconta-6,9,28,31-tetraen-19-yl-4-(dimethylamino) butanoate (DLin-MC3-DMA) was synthesized as described.[99] 3-azido-5-cholestene (**1**) was synthesized as

described.[100] CleanCap eGFP (5moU) mRNA, CleanCap mCherry (5moU) mRNA and CleanCap Cyanine 5 eGFP (5moU) mRNA were purchased from TriLink Biotechnologies (San Diego, CA) or Tebu-bio (Heerhugowaard, The Netherlands).

Liposome Formulation

DOPC liposomes (with and without incorporated Chol-NH-ApoE-peptide, 5 mol%) were formulated in 20 mM HEPES buffer (pH = 7.3) at a total lipid concentration of 5 mM. DOPC and Chol-NH-ApoE-peptide, as stock solutions in chloroform (10mM), were combined to the desired molar ratios and dried to a film, first under a stream of N_2 followed by the removal of trace solvents *in vacuo* for >1 h. Lipid films were hydrated and large unilamellar vesicles formed through extrusion at room temperature (Mini-extruder, Avanti Polar Lipids, Alabaster, US). Hydrated lipids were passed 11 times through a 100 nm polycarbonate (PC) membrane (Nucleopore Track-Etch membranes, Whatman). All liposome dispersions were stored at 4^{o}C and used within 2 days.

Lipid Nanoparticle (LNP) Formulation

Lipid nanoparticles entrapping mRNA were formulated as previously described.[5] In brief, lipid components (MC3, cholesterol, DSPC or DSPG, and PEG-lipid) were dissolved in ethanol. For biodistribution studies, the non-exchangeable tracer DiD or DOPE-LR was added to lipid mixtures at a concentration of 0.1 mol% or 0.2 mol% respectively. The mRNA was dissolved in 25 mM sodium acetate or sodium citrate buffer (pH 4). The two solution were rapidly mixed (N/P ratio of 6) using a T-junction mixer (total flow rate of 20 mL/min, flow rate ratio of 3:1 v/v). The resulting LNP formulation was dialyzed overnight against PBS (pH 7.4), sterile filtered, and concentrated using 10K MWCO centrifugal filters (Amicon® Ultra, Merck). Entrapment efficiency and mRNA concentration were analyzed using the Quant-iT Ribogreen RNA assay (Life Technologies, Burlington, ON). Total lipid concentrations were measured using the Cholesterol E Total-Cholesterol assay (Wako Diagnostics, Richmond, VA). mRNA doses within embryonic zebrafish were calculated using an estimated average weight of 1 mg per embryo, independent of developmental stage, and an injection volume of 1 nl.

LNP and liposome biophysical characterization

LNP and liposome sizes and zeta potentials were measured using a Malvern Zetasizer Nano ZS (software version 7.13, Malvern Panalytical). For DLS (operating wavelength = 633 nm), measurements were carried out at room temperature in 20 mM HEPES buffer (pH = 7.3) for liposomes, and in 1x PBS (pH = 7.4) for LNPs, at a total lipid concentration of approx. 100 µM. Zeta potentials were measured at 500 µM total lipid concentration, using a dip-cell electrode (ZEN1002, Malvern) for liposomes and in a folded capillary cell (DTS1070, Malvern) for LNPs, at room temperature. All reported DLS measurements and zeta potentials are the average of three measurements.

CryoTEM Imaging and Quantification

Vitrification of concentrated (~10 mM) LNPs was performed using a Leica EM GP operating at 21°C and 95% RH. Sample suspensions were placed on glow discharged 100 µm lacey carbon films supported by 200 mesh copper grids (Electron Microscopy Sciences). Optimal results were achieved using a 60 second pre-blot and a 1 second blot time. After vitrification, sample grids were maintained below −170 ◦ C and imaging was performed on a Tecnai T12 (ThermoFisher) with a biotwin lens and LaB6 filament operating at 120 keV equipped with an Eagle 4K x 4K CCD camera (ThermoFisher). Images were acquired at a nominal underfocus of -2 to -3 µm (49,000× magnification) with an electron dose of ~2000 e^{-}·nm^{-2}. Images were processed and particle size was quantified using the Fiji distribution of ImageJ.[101] For quantification, particle sizes were determined on particles present in amorphous vitrified water and obtained from a triplicate of assemblies (~150-200 particles per assembly per formulation). Generation of frequency distribution graphs was performed using GraphPad Prism (v 6.0).

Zebrafish Husbandry and Injections

Zebrafish (*Danio rerio*, strain *AB/TL*) were maintained and handled according to the guidelines from the Zebrafish Model Organism Database (http://zfin.org) and in compliance with the directives of the local animal welfare committee of Leiden University. Fertilization was performed by natural spawning at the beginning of the light period, and eggs were raised at 28.5 °C in egg water (60 µg/ mL Instant Ocean sea salts). In addition to wild-type (*AB/TL*) embryos, previously established Tg(*mpeg1*:mCherry)^{gl23} [102] and *stab2*^{ibl2}*stab1*^{ibl3} [51] (described in **Chapter 3**) zebrafish lines were also used in this study.

Fluorescently labelled LNPs were injected into 54-96 hours post fertilization (hpf) zebrafish embryos using a modified microangraphy protocol.[103] Embryos were anesthetized in 0.01% tricaine and embedded in 0.4% agarose containing tricaine before injection. To improve reproducibility of microangiography experiments, 1 nl volume were calibrated and injected into the common cardinal vein (2-3 dpf) or primary head sinus (4 dpf). A small injection space was created by penetrating the skin with the injection needle and gently pulling the needle back, thereby creating a small pyramidal space in which the liposomes or LNPs were injected. Successfully injected embryos were identified through the backward translocation of venous erythrocytes and the absence of damage to the yolk ball. Selected zebrafish embryos successfully injected were kept in egg water at 28.5 degrees until later imaging (1.5 or 24 hours post injection).

Zebrafish confocal imaging acquisition and processing

Zebrafish embryos were randomly picked from a dish of 10-30 successfully injected embryos to be imaged after 1.5 or 24 h post injection (hpi). Confocal z-stacks were captured on a Leica TCS SPE or SP8 confocal microscope, using a 10x air objective (HCX PL FLUOTAR), a 40x water-immersion objective (HCX APO L) or 63x water-immersion objective (HC PL APO CS). For whole-embryo views, 3 or 4 overlapping z-stacks were captured to cover the complete body. Laser intensity, gain and offset settings were identical between stacks and when comparing samples per experiment. Images were processed using the Fiji distribution of ImageJ.[101] Confocal image stacks (raw data) are available upon reasonable request.

Mouse husbandry, injection protocol and cell isolation

All mouse protocols were approved by the Canadian Animal Care Committee and conducted in accordance with relevant guidelines and regulations. Mice were maintained on a regular 12-hour light/12- hour dark cycle in a specific pathogen-free animal facility at UBC. C57Bl6 male mice aged between 8 to 10 weeks were used throughout. These mice were divided into groups of 2 and either received intravenous (*i.v*) injection of LNP-mRNAs (either DSPC-LNPs or srLNPs) or PBS as a negative control. For biodistribution studies, LNPs entrapping luciferase mRNA were labelled with 0.5 mol% DiD as fluorescent lipid marker. Injections were performed at 42.75 mg/kg total lipid and mice were sacrificed at 2 hpi. For gene expression studies, LNPs encapsulating mRNA coding for the fluorescent reporter gene mCherry were used, injections were performed at 0.25 mg/kg mRNA dose, and mice were sacrificed at 24 hpi. Mice were anesthetized using a

high dose of isofluorane followed by CO_2. Trans-cardiac perfusion was performed as follows: once the animals were unresponsive, a 5 cm medial incision was made through the abdominal wall, exposing the liver and heart. While the heart was still beating, a butterfly needle connected to a 30 mL syringe loaded with pre-warmed Hank's Balanced Salt Solution (HBSS, Gibco) was inserted into the left ventricle. Next, the liver was perfused with perfusion medium (HBSS, supplemented with 0.5 mM EDTA, Glucose 10 mM and HEPES 10 mM) at a rate of 3 mL/min for 10 min. Once liver swelling was observed, a cut was performed on the right atrium and perfusion was switched to digestion medium (DMEM, Gibco supplemented with 10% fetal bovine serum (FBS, Gibco) and 1% penicillin streptomycin (Gibco) and 0.8 mg/mL Collagenase Type IV, Worthington) at 3 mL/min for another 10 min. At the end of the perfusion of the entire system, as determined by organ blanching, the whole liver and spleen were dissected and transferred to 50 mL Falcon tubes containing 10 ml ice cold (4°C) perfusion media and placed on ice. Next, isolation of hepatic cell types (*i.e.* hepatocytes, Kupffer cells (KCs) and liver sinusoid endothelial cells (LSECs)) was performed following density gradient-based separation. Briefly, the liver was transferred to a Petri dish containing digestion medium, minced under sterile conditions, and incubated for 20 min at 37°C with occasional shaking of the plate. Cell suspensions were then filtered through a 40 µm mesh cell strainer to eliminate any undigested tissue remnants. Primary hepatocytes were separated from other liver residing cells (LRCs) by low-speed centrifugation at 500 rpm with no brake. The supernatant containing mainly LRCs was pelleted using low speed (3000 rpm) centrifugation at 4°C, aliquoted and washed twice with ice cold PBS containing 2% FBS. The pellet containing mainly hepatocytes was collected, washed at low speed and placed on ice. Phenotypic detection using monoclonal antibodies, assessment of LNP delivery and mRNA expression on liver cells was performed immediately after isolation to avoid changes in gene regulation, polarization and dedifferentiation.[104] LNP biodistribution across individual RES cell types of the spleen (*i.e.* endothelial cells and macrophages) were also characterized. Here, the spleen was also dissected and placed into a 40 µm mesh cell and mashed through the cell strainer into the petri dish using the plunger end of the syringe. The suspended cells were transferred to a 15 mL Falcon tube and centrifuged at 1000 rpm for 5 minutes. The pellet was resuspended in 1 mL ACK lysis buffer (Invitrogen) to lyse the red blood cells, aliquoted in FACS buffer and stained with antibodies as described below to identify splenic endothelial cells and macrophages.

FACS analysis

Cell aliquots were resuspended in 300 µl FACS staining buffer (FBS 2%, Sodium Azide 0.1% and ethylenediaminetetraacetic acid (EDTA 1mM)) followed by staining with fluorescence tagged antibodies. Prior to staining, cells were first labeled with anti-mouse CD16/CD32 (mouse Fc blocker, Clone 2.4G2) (AntibodyLab, Vancouver, Canada) to reduce background. Hepatocytes were detected following staining with primary mouse antibody detecting ASGR1 (8D7, Novus Biologicals) followed by goat polyclonal secondary antibody to mouse IgG2a labeled to PE-Cy7 (BioLegend). Kupffer cells were detected with CD11b – FITC or PE (Invitrogen) and F4/80high labeled to APC, endothelial cells with rabbit polyclonal CD31-PE-Cy7 (Abcam) and LSECs identified with CD146-VioBlue (Miltenyi Biotec) and CD31-PE-Cy7. Spleen macrophages and endothelial cells were detected using appropriate antibodies and identified as CD11bhigh and CD31+ve cells following antibody labeling as described. The data were acquired using a LSRII flow cytometer and the FACSDiva software and analyzed by FlowJo following acquisition of at least 10,000 events after gating on viable cell populations. LNP-mRNA delivery or transfection efficacy were assessed based on the relative mean fluorescence intensity of DiD or mCherry positive cells, respectively, measured on histograms obtained from gated cell populations.

6.6 Abbreviations

acLDL	acetylated low-density lipoprotein
apoE	apolipoprotein E
CCMV VLP	cowpea chlorotic mottle virus derived virus-like particles
CHT	caudal hematopoietic tissue
CryoTEM	cryo-electron transmission microscope
CCV	common cardinal vein
CV	cardinal vein
dpf	days post fertilization
DA	dorsal aorta
DLAV	dorsal longitudinal anastomotic vessel
DMG-PEG2k	1,2-dimyristoyl-rac-glycero-3-methoxypolyethyleneglycol-2k
DOPC	1,2-dioleyl-sn-glycerol-3-phosphocholine
DSPG	1,2-disteraroyl-*sn*-glycero-3-phospho-glycerol
DSPC	1,2-distearoyl-*sn*-glycero-3-phosphocholine
ECs	endothelial cells
fluoHA	fluorescently labeled hyaluronic acid
hpi	hour(s) post injection
i.m.	intramuscularly
ISV	intersegmental vessels
i.v.	intravenously
KCs	Kupffer cells
LDLR	low density lipoprotein receptor
L-FABP	liver fatty acid binding protein
LNPs	lipid nanoparticles
LRP	low-density lipoprotein receptor-related proteins
LSECs	liver sinusoidal endothelial cells
MPS	mononuclear phagocyte system
OxLDL	oxidized low-density lipoprotein
PCV	posterior cardinal vein
PHS	primitive head sinus
RES	reticuloendothelial system
RNAi	RNA interference
srLNPs	scavenger receptor lipid nanoparticles
SECs	scavenging endothelial cells
siRNA	silencing RNA
TTR	transthyretin

6.7 Supporting Information

Supplementary Table 1. Composition, size (as measured by DLS), polydispersity (PDI), surface charge (as measured by zeta potential), RNA encapsulation efficiency (as measured by RiboGreen assay) and reproducibility of all LNP and liposome formulations used in this study.

Formulation	mRNA	Fluorescent lipid	% of Fluorescent Lipid	Avg. Size (nm)	PDI	Zeta Potential (mV)	EE (%)	n
DSPC-LNP	eGFP	DOPE-LR	0.2	82.5 ± 2.0	0.085 ± 0.027	-5.5 ± 1.2	95 ± 2	3
srLNP	eGFP	DOPE-LR	0.2	89.2 ± 5.7	0.094 ± 0.023	-21.9 ± 2.5	88 ± 3	3
DSPC-LNP	eGFP	DiD	0.1	82.5 ± 3.4	0.081 ± 0.026	-4.1 ± 1.6	95 ± 1	3
srLNP	eGFP	DiD	0.1	94.7 ± 4.0	0.102 ± 0.016	-17.5 ± 2.4	91 ± 2	3
DSPC-LNP	eGFP	-	-	82.5 ± 4.0	0.103 ± 0.037	-4.0 ± 0.9	93 ± 1	2
srLNP	eGFP	-	-	86.6 ± 6.7	0.108 ± 0.006	-19.0 ± 1.1	91 ± 4	2
DSPC-LNP	mCherry	DiD	0.1	79.9 ± 5.2	0.072 ± 0.038	-3.7 ± 1.8	94 ± 3	2
srLNP	mCherry	DiD	0.1	92.7 ± 3.5	0.102 ± 0.012	-18.8 ± 2.1	89 ± 4	2
DSPC-LNP	Cy5-mRNA	DOPE-LR	0.2	87.0 ± 3.5	0.090 ± 0.016	-3.9 ± 0.9	95 ± 3	2
srLNP	Cy5-mRNA	DOPE-LR	0.2	94.1 ± 2.3	0.096 ± 0.01	-16.2 ± 1.2	91 ± 2	2
DOPC	-	DOPE-LR	0.2	96.3 ± 4.0	0.095 ± 0.011	-6.1 ± 1.1	-	2
DOPC+ApoE-peptide	-	DOPE-LR	0.2	104.7 ± 3.8	0.075 ± 0.012	14.7 ± 1.6	-	2

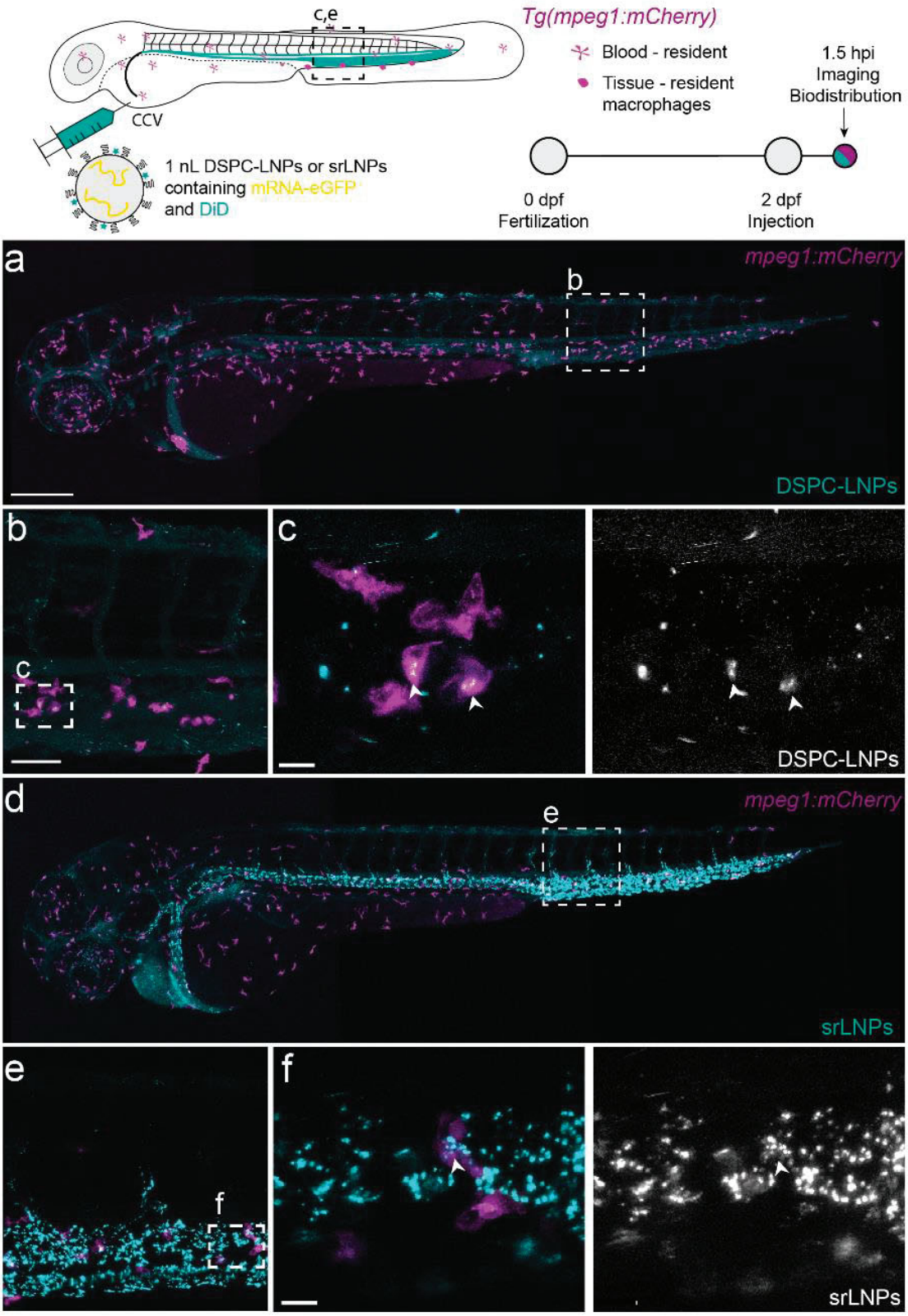

Supplementary Figure 1. Biodistribution of DSPC-LNPs and srLNPs in transgenic *mpeg1:*mCherry zebrafish embryos at 1.5 hpi. Schematic showing the site of LNP injection *(i.v)* within the embryonic zebrafish (2 dpf) and imaging timeframe. LNPs contained DiD (cy5, 0.1 mol%) as fluorescent lipid probe and unlabeled eGFP mRNA.

Tg(*mpeg1:*mCherry*)* zebrafish embryos stably expressing mCherry (magenta) within all macrophages. *Injected dose*: ~10 mM lipid, ~0.2 mg/kg mRNA. *Injection volume*: 1 nl. CCV, common cardinal vein **(a)** Whole embryo view (10x magnification), **(b)** tissue level view (40x magnification) and **(c)** a zoom of a projection of three confocal z-stacks, showing fluorescent co-localisation of DiD (LNP probe) and transgenic mCherry (white arrowheads), confirming low-level DSPC-LNP uptake within these cells. **(d)** Whole embryo view (10x magnification), **(e)** tissue level view (40x magnification) and **(f)** a zoom of a projection of three confocal z-stacks, showing fluorescent colocalisation of DiD (LNP probe) and transgenic mCherry (white arrowheads), confirming simultaneous uptake of srLNPs within both SECs and blood resident macrophages. Scale bars: 200 µm (whole body), 50 µm (tissue level), 10 µm (zoom).

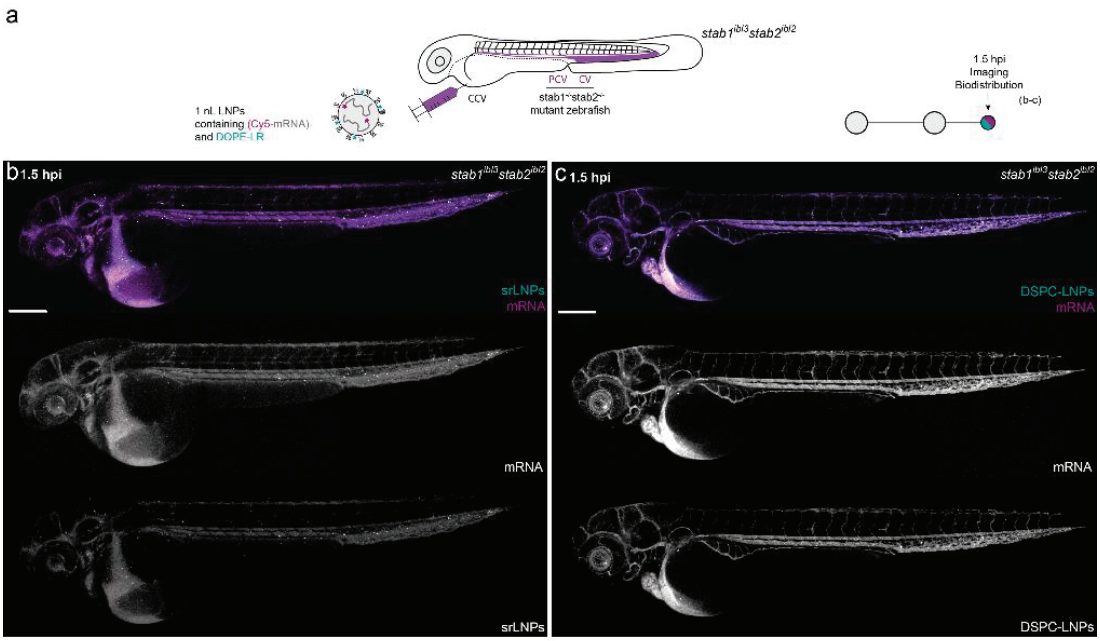

Supplementary Figure 2. Biodistribution of srLNPs and DSPC-LNPs in double knock-out (stab1$^{-/-}$/stab2$^{-/-}$) mutant embryos at 1.5 hpi. **(a)** Schematic showing the site of LNP injection (*i.v*) within double knockout (*stab1^{ibl3}-stab2^{ibl2}*)[51] (described in **Chapter 3**) zebrafish embryos (2 dpf) and imaging timeframe. LNPs contained DOPE-LR (cyan, 0.2 mol%) as fluorescent lipid probe and Cy5-labelled eGFP mRNA (magenta) as fluorescent mRNA probe. Injected dose: ~10 mM lipid, ~0.2 mg/kg mRNA. Injection volume: ~1 nl. CV – cardinal vein; PCV – posterior cardinal vein; CCV – common cardinal vein. **(b,c)** Whole embryo (10x magnification) views of srLNP and DSPC-LNP biodistribution within stab1$^{-/-}$/stab2$^{-/-}$ mutant embryos (2 dpf) at 1.5 hpi. In both cases, LNPs were mostly freely circulating throughout the vasculature of the embryo at 1.5 hpi. Scale bar: 200 µm.

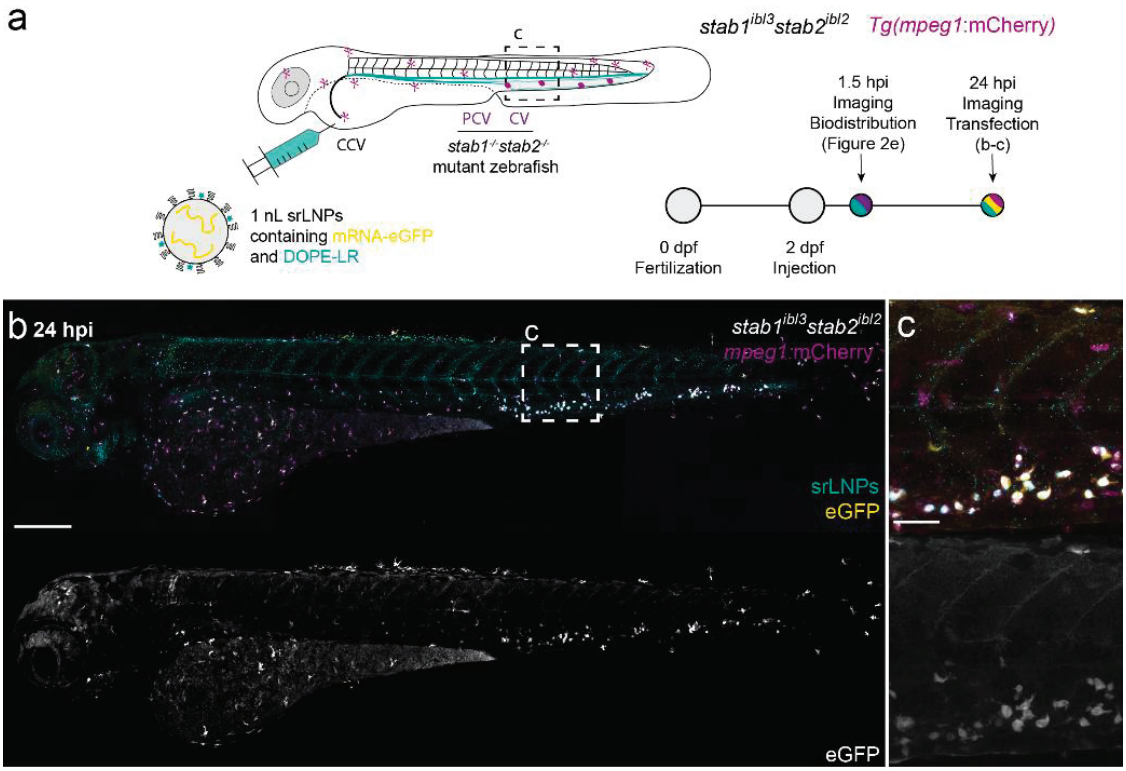

Supplementary Figure 3. srLNP biodistribution and eGFP expression in double knock-out (stab1$^{-/-}$ stab2$^{-/-}$) mutant embryos at 24 hpi. (a) Schematic showing the site of LNP injection (*i.v*) within Tg(*mpeg1*:mCherry), double knockout (*stab1*^{ibl3}*stab2*^{ibl2}) [51] (described in **Chapter 3**) zebrafish embryos (2 dpf) and imaging timeframe. LNPs contained DiD (cy5, 0.1 mol%, cyan) as fluorescent lipid probe and unlabeled eGFP mRNA. Injected dose: ~10 mM lipid, ~0.2 mg/kg mRNA. Injection volume: ~1 nl. CCV – common cardinal vein, CV – cardinal vein; PCV – posterior cardinal vein. **(b,c)** Whole embryo (10x magnification) and tissue level (40x magnification) views of srLNP biodistribution and eGFP expression within stab1$^{-/-}$/stab2$^{-/-}$ mutant embryos at 24 hpi. Within these embryos, srLNP localisation and eGFP expression is observed within blood resident macrophages (magenta) but not SECs at 24 hpi. Scale bars: 200 µm (whole embryo) and 50 µm (tissue level).

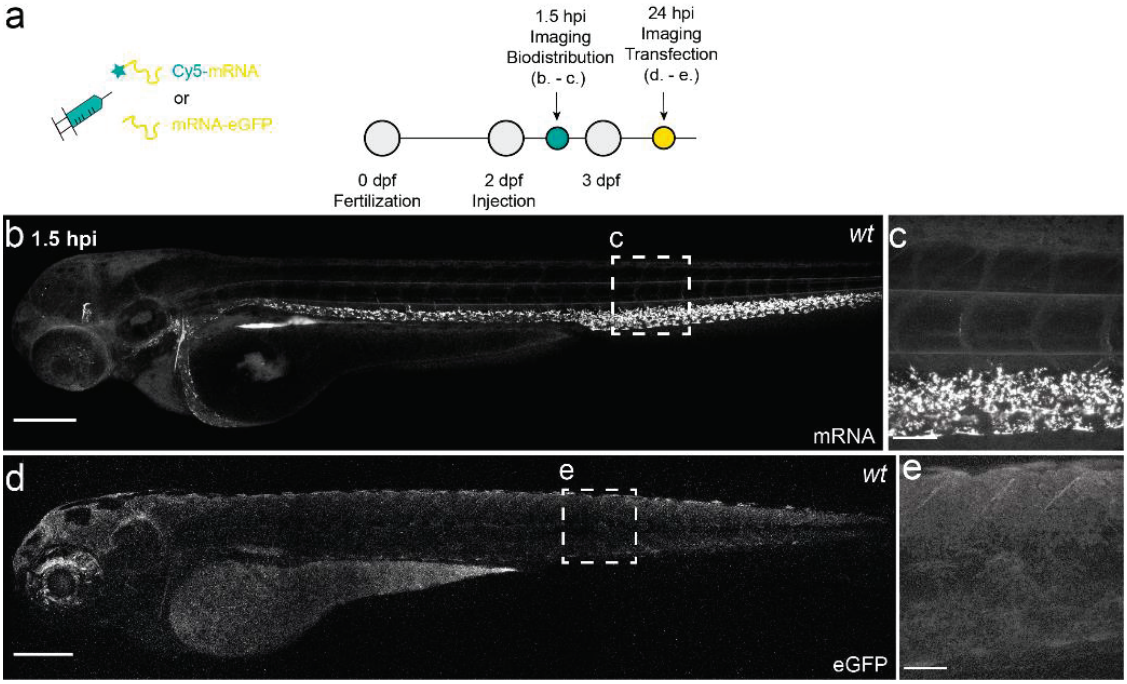

Supplementary Figure 4. Biodistribution and expression of free eGFP mRNA in wildtype (*AB/TL*) embryonic zebrafish. (a) Schematic showing the site of free mRNA injection (*i.v.*; 0.2 mg/kg, 1 nL) within embryonic zebrafish (2 dpf) and imaging timeframe. CCV – common cardinal vein. **(b,c)** Whole embryo (10x magnification) and tissue level (40x magnification) views of free mRNA (cy5-labelled) biodistribution at 1.5 hpi. Free mRNA primarily accumulated within SECs of the embryonic zebrafish at 1.5 hpi, likely mediated by Stabilin receptors.[59] Any phagocytotic uptake of free mRNA within blood resident macrophages cannot be clearly defined within the CHT of the wild-type embryo given the high fluorescence signal (cy5) within overlapping SECs. **(d,e)** Whole embryo (10x magnification) and tissue level (40x magnification) views of eGFP expression (unlabeled mRNA) at 24 hpi. No significant eGFP expression is observed within SECs or blood resident macrophages of the embryonic fish. Scale bars: 200 µm (whole embryo) and 50 µm (tissue level).

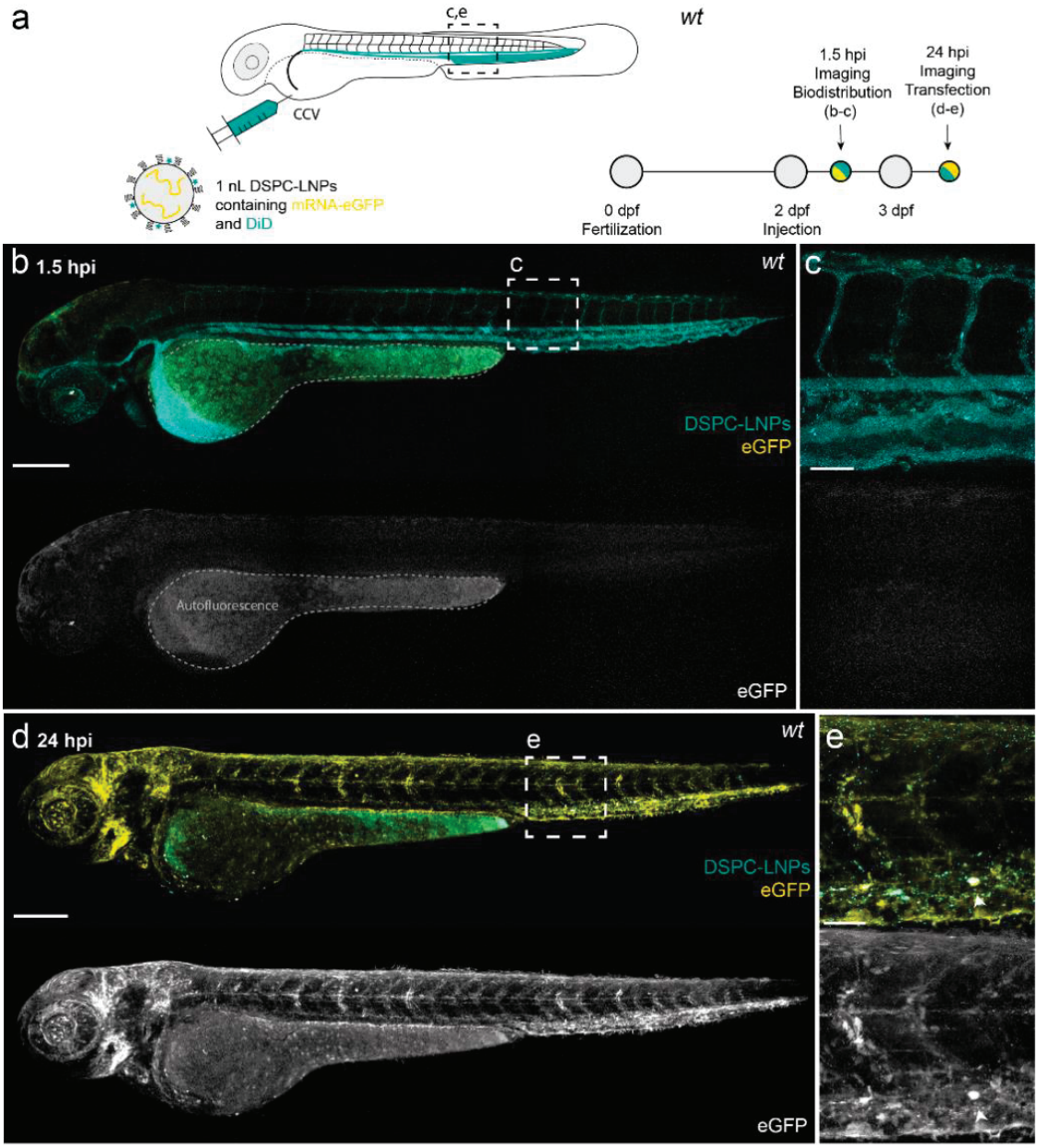

Supplementary Figure 5. DSPC-LNP biodistribution and eGFP expression within wild-type (*AB/TL*) zebrafish embryos at 1.5 and 24 hpi. (a) Schematic showing the site of DSPC-LNPs (*i.v.*) injection within embryonic zebrafish (2 dpf) and imaging timeframe. DSPC-LNPs contained DiD (cy5, 0.1 mol%) as fluorescent lipid probe and unlabelled eGFP mRNA (capped) payload. Injected dose: ~10 mM lipid, ~0.2 mg/kg mRNA. Injection volume: ~1 nl **(b,c)** Whole embryo (10x magnification) and tissue level (40x magnification) views of DSPC-LNP biodistribution and eGFP expression within the embryonic zebrafish at 1.5 hpi. DSPC-LNPs were mostly freely circulating, confined to and homogenously distributed throughout the vasculature of the embryo at 1.5 hpi. Low level embryo autofluorescence (GFP channel) within the yolk sac and pigment cells of the embryo is highlighted. **(d,e)** Whole embryo and tissue level views of DSPC-LNP biodistribution and eGFP expression within the embryonic zebrafish at 24 hpi. eGFP

expression within macrophages (based on location and morphology) highlighted with white arrowheads. Scale bars: 200 µm (whole embryo) and 50 µm (tissue level).

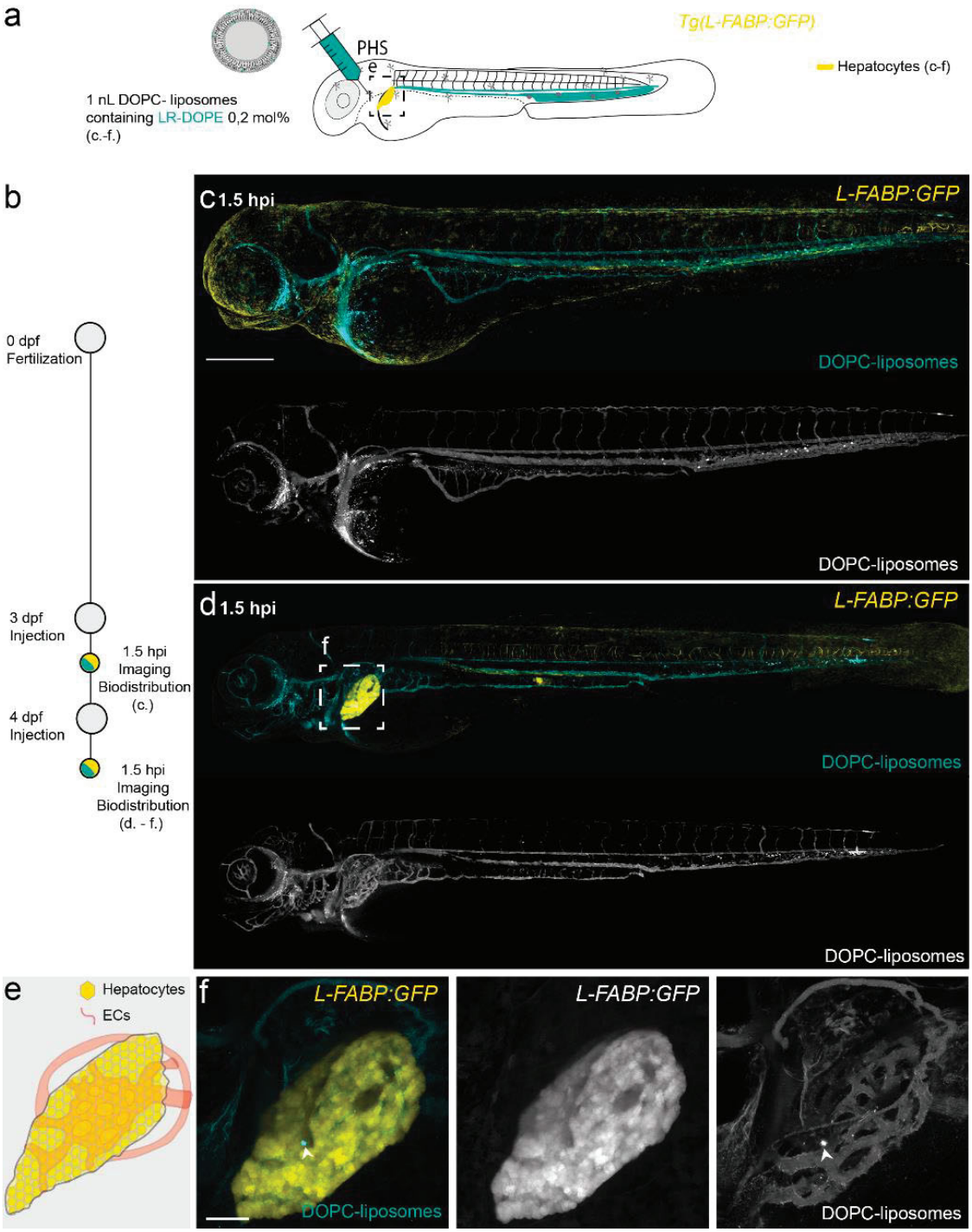

Supplementary Figure 6. DOPC liposome biodistribution in *L-FABP*:eGFP transgenic zebrafish embryos (3 and 4 dpf) at 1.5hpi. (a) Schematic showing the site of liposome injection (*i.v.*) within embryonic zebrafish (3 or 4 dpf). Liposomes contained 0.2 mol% DOPE-LR as fluorescent lipid probe (cyan). Injected dose: ~5 mM lipid. Injection volume: 1 nl. Tg(*LFABP:*eGFP) zebrafish embryos expressing eGFP (yellow) in hepatocytes. PHS – primary head sinus. **(b)** Injection and imaging timeframe. **(c,d)** Whole embryo (10x

magnification) views of DOPC liposome biodistribution within the embryonic zebrafish (3 or 4 dpf) at 1.5 hpi. **(e)** Tissue level schematic of the embryonic liver at 4 dpf. **(f)** Tissue level (40x magnification) views of DOPC liposome biodistribution within the liver of a four-day old embryo. Liposomes freely circulate throughout the liver vasculature and do not associate with either ECs or hepatocytes of the embryonic liver. The single, intense fluorescent (DOPE-LR) punctum (white arrowhead) observed within the liver of the four-day old embryo is most likely due to macrophage uptake. Scale bars: 200 µm (whole embryo) and 50 µm (tissue level).

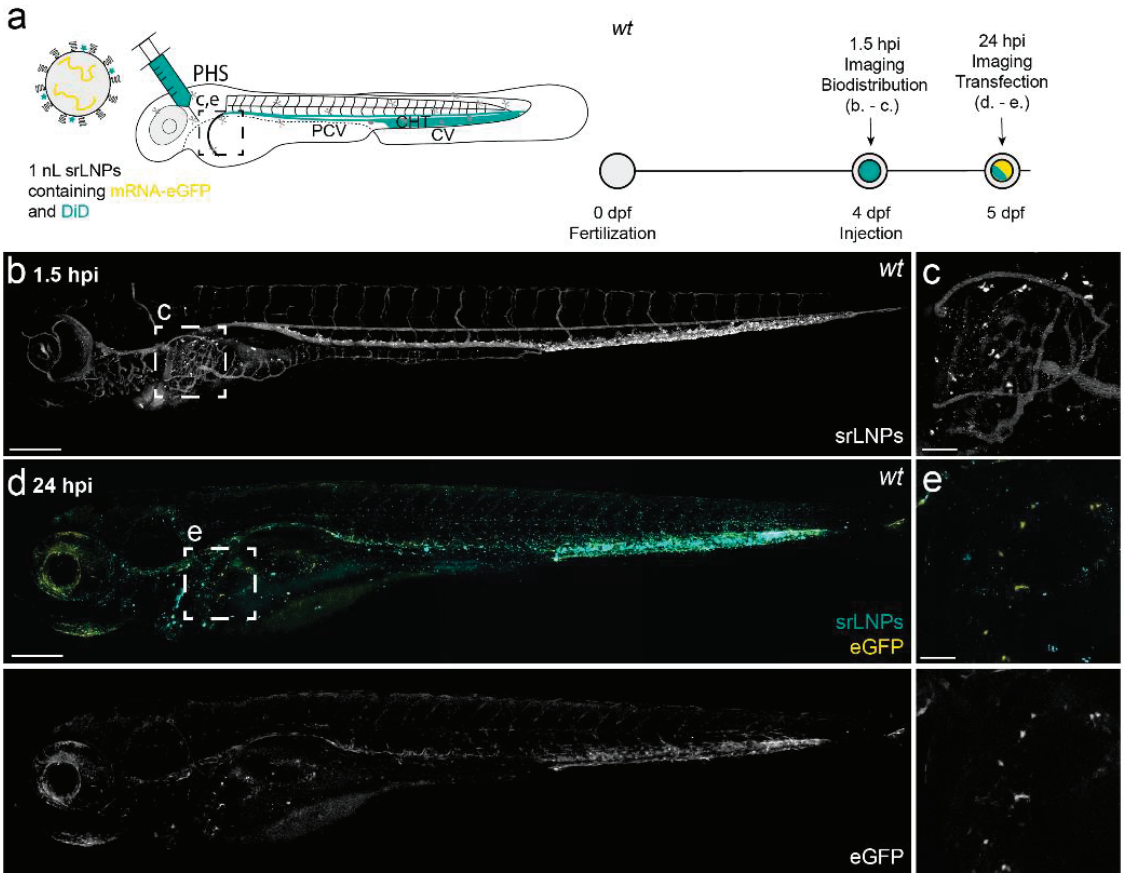

Supplementary Figure 7. srLNP (30mM) biodistribution and mRNA expression within wildtype (*AB/TL*) embryonic zebrafish. (a) Schematic showing the site of srLNP injection (*i.v.*) within embryonic zebrafish (4 dpf). srLNPs contained DiD (approx. 0.1 mol%) as fluorescent lipid probe and unlabeled, eGFP mRNA (capped) payload. Injection and imaging timeframe. Injected dose: ~10 mM lipid, ~0.2 mg/kg mRNA. Injection volume: 1 nl. PHS – primary head sinus. **(b,c)** Whole embryo (10x magnification) and tissue level (40x magnification, liver region) views of srLNP biodistribution (DiD, cyan) at 1.5 hpi. srLNPs were mainly associated with SECs within the PCV, CV and CHT of the four-day old embryo at 1.5 hpi. Due to the higher injected dosage, a significant fraction of srLNPs are also observed in circulation, possibly due to saturation of Stabilin receptors. Within the liver region, individual fluorescent punctae associated with srLNP accumulation are most likely due to macrophage uptake. **(d,e)** Whole embryo (10x magnification) and tissue level (40x magnification, liver region) views of srLNP biodistribution and eGFP expression within the embryonic zebrafish at 24 hpi. srLNPs remain predominantly localized within the PCV, CV and CHT at 24 hpi, with exogenous

eGFP expression mainly restricted to this region of the five day-old embryo. Within the liver region, eGFP fluorescence is restricted to a handful of individual cells and does not evidently colocalize with srLNP-associated fluorescence (DiD). From these images, it is not clear whether eGFP fluorescence within the liver is due to macrophage uptake (possibly distal from the liver, and following macrophage migration), embryo autofluorescence or uptake within an alternative cell type. Scale bars: 200 µm (whole embryo) and 50 µm (tissue level).

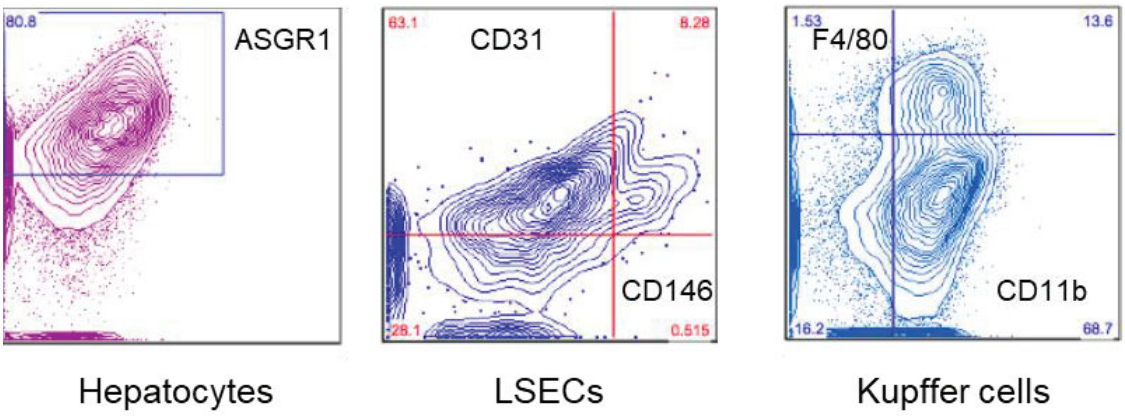

Supplementary Figure 8. Detection of major cell types in the liver microenvironment. Representative flow cytometry density plots illustrate the detection of specific hepatic cell types following liver perfusion and cell harvesting.

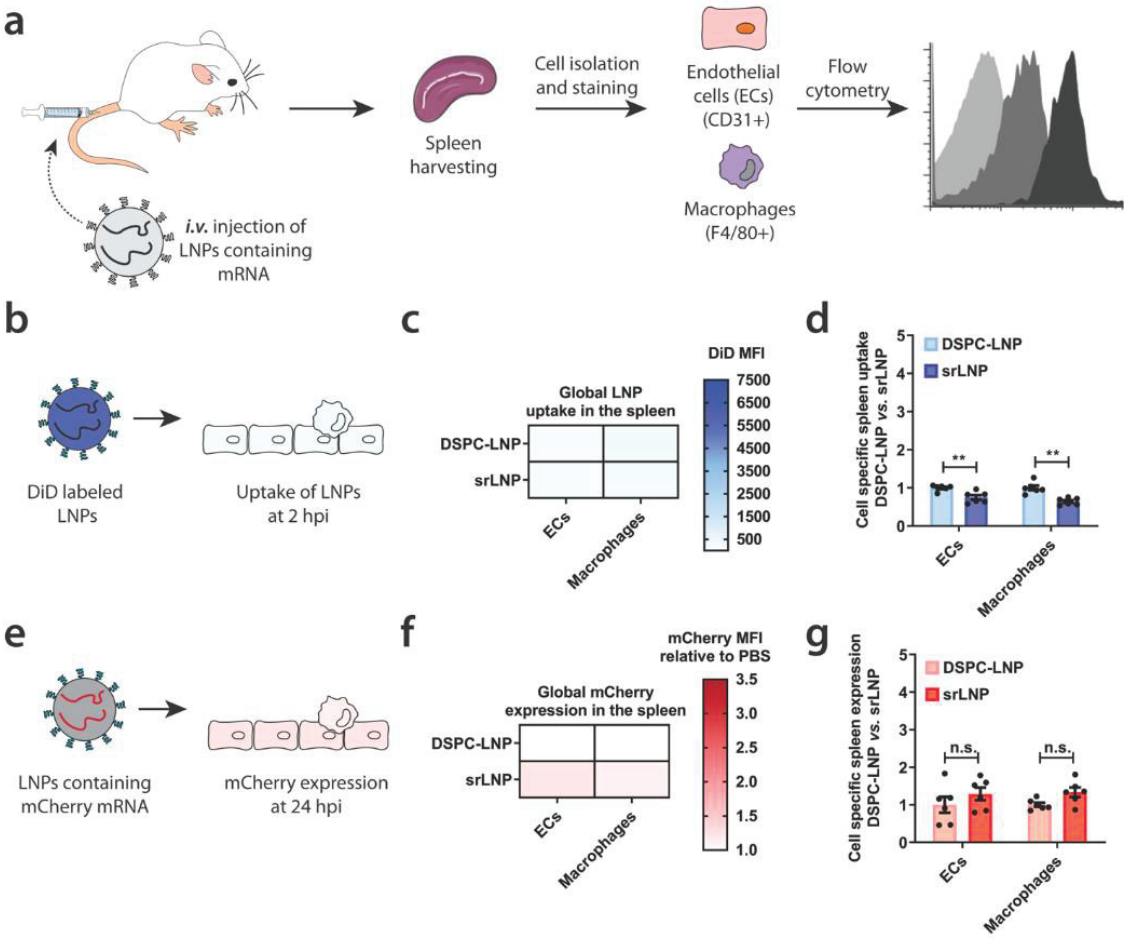

Supplementary Figure 9. LNP uptake and functional mRNA delivery within different splenic cell types. (a) Schematic illustrating the procedure to isolate different splenic cell types and determine LNP-mRNA targeting and functional mRNA delivery. Following intravenous LNP injection (*i.v*), splenic cells were isolated and stained with specific antibodies (in parentheses), and flow cytometry used to analyze LNP uptake or gene expression. **(b)** For biodistribution studies, LNPs contained DiD (0.5 mol%) as fluorescent probe. Cellular uptake of DSPC-LNP and srLNP was assessed 2 hpi. Injected dose: 42.75 mg/kg total lipid. **(c)** Heatmap of global LNP uptake in the spleen determined by absolute DiD fluorescence. **(d)** Cell specific spleen uptake normalized to DSPC-LNP for each cell type. **(e)** For gene expression experiments, LNPs contained mCherry-mRNA. Functional mRNA delivery was assessed based on mCherry reporter gene expression levels at 24 hpi. **(f)** Heatmap of mCherry expression in different spleen cell types using DSPC-LNP or srLNP. Injected dose: 0.25 mg/kg mRNA. srLNP show no significant mCherry expression compared to DSPC-LNP in splenic RES cells. **(g)** Cell specific mCherry expression normalized to DSPC-LNP for each cell type. In all cases, n = 6 represents 3 separate spleen tissue samples from 2 mice sorted into individual cell types. Bars and error bars in **c** represent mean ± s.e.m. The data was normalized to the average expression of DSPC-LNPs within each cell type. Statistical significance was evaluated using a two-tailed unpaired Student's t-test. n.s. = not significant, ** $p < 0.01$, *** $p < 0.001$. Exact P values for **d**: ECs P= 0.0039, Macrophages P= 0.0011. Exact P values for **g**: ECs P= 0.308, Macrophages P= 0.074.

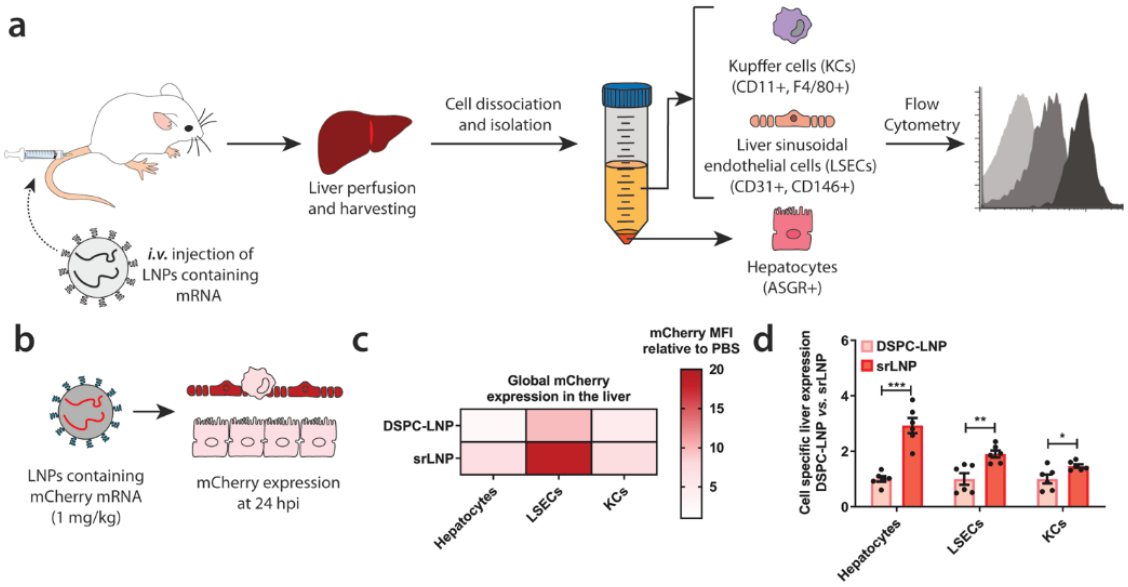

Supplementary Figure 10. Functional mCherry mRNA delivery to hepatic RES cell types at an injected mRNA dose of 1 mg/kg. (a) Schematic illustrating the procedure to isolate different hepatic cell types and determine LNP-mRNA targeting and functional mRNA delivery. Following intravenous LNP injection (*i.v*) the liver was perfused with collagenase IV, hepatic cells were isolated and stained with specific antibodies, and flow cytometry was used to analyze LNP uptake and gene expression. Specific antibody markers used to uniquely identify hepatocytes, LSECs and KCs, respectively, are defined in parentheses. **(b)** LNPs contained mCherry-mRNA. Functional mRNA delivery was assessed based on mCherry reporter gene expression levels at 24 hpi. **(c)** Heatmap of mCherry expression in different liver cell types enabled by mRNA delivery using DSPC-LNP and srLNP. Injected dose: 1 mg/kg mRNA. srLNPs led to enhanced gene expression in hepatic RES cells, predominantly in LSECs. **(d)** Cell specific mCherry expression normalized to DSPC-LNP for each cell type. In all cases, n = 6 represents 3 separate liver tissue samples from 2 mice sorted into individual cell types. Bars and error bars in c and e represent mean ± s.e.m. Statistical significance was evaluated using a two-tailed unpaired Student's t-test. * $p < 0.05$, ** $p < 0.01$, *** $p < 0.001$. Exact P values for **d**: Hepatocytes P= 0.00018, LSECs P= 0.0083, KCs P= 0.025.

6.8 References

1. Delivering the promise of RNA therapeutics. *Nature Medicine* **2019,** *25* (9), 1321-1321.
2. Dammes, N.; Peer, D., Paving the Road for RNA Therapeutics. *Trends in Pharmacological Sciences* **2020,** *41* (10), 755-775.
3. Yin, H.; Kanasty, R. L.; Eltoukhy, A. A.; Vegas, A. J.; Dorkin, J. R.; Anderson, D. G., Non-viral vectors for gene-based therapy. *Nature Reviews Genetics* **2014,** *15* (8), 541-555.
4. Cullis, P. R.; Hope, M. J., Lipid Nanoparticle Systems for Enabling Gene Therapies. *Molecular Therapy* **2017,** *25* (7), 1467-1475.
5. Kulkarni, J. A.; Witzigmann, D.; Chen, S.; Cullis, P. R.; van der Meel, R., Lipid Nanoparticle Technology for Clinical Translation of siRNA Therapeutics. *Accounts of Chemical Research* **2019,** *52* (9), 2435-2444.
6. Akinc, A.; Maier, M. A.; Manoharan, M.; Fitzgerald, K.; Jayaraman, M.; Barros, S.; Ansell, S.; Du, X.; Hope, M. J.; Madden, T. D.; Mui, B. L.; Semple, S. C.; Tam, Y. K.; Ciufolini, M.; Witzigmann, D.; Kulkarni, J. A.; van der Meel, R.; Cullis, P. R., The Onpattro story and the clinical translation of nanomedicines containing nucleic acid-based drugs. *Nature Nanotechnology* **2019,** *14* (12), 1084-1087.
7. Adams, D.; Gonzalez-Duarte, A.; O'Riordan, W. D.; Yang, C. C.; Ueda, M.; Kristen, A. V.; Tournev, I.; Schmidt, H. H.; Coelho, T.; Berk, J. L., et al., Patisiran, an RNAi therapeutic, for hereditary transthyretin amyloidosis. *New England Journal of Medicine* **2018,** *379* (1), 11-21.
8. Kumar, V.; Qin, J.; Jiang, Y.; Duncan, R. G.; Brigham, B.; Fishman, S.; Nair, J. K.; Akinc, A.; Barros, S. A.; Kasperkovitz, P. V., Shielding of Lipid Nanoparticles for siRNA Delivery: Impact on Physicochemical Properties, Cytokine Induction, and Efficacy. *Molecular therapy. Nucleic acids* **2014,** *3* (11), e210-e210.
9. Mui, B. L.; Tam, Y. K.; Jayaraman, M.; Ansell, S. M.; Du, X.; Tam, Y. Y. C.; Lin, P. J.; Chen, S.; Narayanannair, J. K.; Rajeev, K. G.; Manoharan, M.; Akinc, A.; Maier, M. A.; Cullis, P.; Madden, T. D.; Hope, M. J., Influence of Polyethylene Glycol Lipid Desorption Rates on Pharmacokinetics and Pharmacodynamics of siRNA Lipid Nanoparticles. *Molecular therapy. Nucleic acids* **2013,** *2* (12), e139-e139.
10. Akinc, A.; Querbes, W.; De, S.; Qin, J.; Frank-Kamenetsky, M.; Jayaprakash, K. N.; Jayaraman, M.; Rajeev, K. G.; Cantley, W. L.; Dorkin, J. R., et al., Targeted delivery of RNAi therapeutics with endogenous and exogenous ligand-based mechanisms. *Molecular Therapy* **2010,** *18* (7), 1357-1364.
11. Nguyen, J.; Szoka, F. C., Nucleic acid delivery: the missing pieces of the puzzle? *Accounts of chemical research* **2012,** *45* (7), 1153-1162.
12. Sato, Y.; Matsui, H.; Yamamoto, N.; Sato, R.; Munakata, T.; Kohara, M.; Harashima, H., Highly specific delivery of siRNA to hepatocytes circumvents endothelial cell-mediated lipid nanoparticle-associated toxicity leading to the safe and efficacious decrease in the hepatitis B virus. *Journal of Controlled Release* **2017,** *266* (September), 216-225.
13. DeRosa, F.; Guild, B.; Karve, S.; Smith, L.; Love, K.; Dorkin, J. R.; Kauffman, K. J.; Zhang, J.; Yahalom, B.; Anderson, D. G.; Heartlein, M. W., Therapeutic efficacy in a hemophilia B model using a biosynthetic mRNA liver depot system. *Gene therapy* **2016,** *23* (10), 699-707.
14. Ramaswamy, S.; Tonnu, N.; Tachikawa, K.; Limphong, P.; Vega, J. B.; Karmali, P. P.; Chivukula, P.; Verma, I. M., Systemic delivery of factor IX messenger RNA for protein replacement therapy. *Proceedings of the National Academy of Sciences of the United States of America* **2017,** *114* (10), E1941-E1950.
15. Chen, S.; Tam, Y. Y. C.; Lin, P. J. C.; Leung, A. K. K.; Tam, Y. K.; Cullis, P. R., Development of lipid nanoparticle formulations of siRNA for hepatocyte gene silencing following subcutaneous administration. *Journal of Controlled Release* **2014,** *196*, 106-112.
16. Sago, C. D.; Lokugamage, M. P.; Islam, F. Z.; Krupczak, B. R.; Sato, M.; Dahlman, J. E., Nanoparticles That Deliver RNA to Bone Marrow Identified by in Vivo Directed Evolution. *Journal of the American Chemical Society* **2018,** *140* (49), 17095-17105.
17. Lokugamage, M. P.; Sago, C. D.; Gan, Z.; Krupczak, B. R.; Dahlman, J. E., Constrained Nanoparticles Deliver siRNA and sgRNA to T Cells In Vivo without Targeting Ligands. *Advanced Materials* **2019,** *31* (41), 1902251-1902251.
18. Paunovska, K.; Gil, C. J.; Lokugamage, M. P.; Sago, C. D.; Sato, M.; Lando, G. N.; Gamboa Castro, M.; Bryksin, A. V.; Dahlman, J. E., Analyzing 2,000 in vivo Drug Delivery Data Points Reveals Cholesterol Structure Impacts Nanoparticle Delivery. *ACS Nano* **2018,** *12*, 8341-8349.

19. Paunovska, K.; Da Silva Sanchez, A. J.; Sago, C. D.; Gan, Z.; Lokugamage, M. P.; Islam, F. Z.; Kalathoor, S.; Krupczak, B. R.; Dahlman, J. E., Nanoparticles Containing Oxidized Cholesterol Deliver mRNA to the Liver Microenvironment at Clinically Relevant Doses. *Advanced materials (Deerfield Beach, Fla.)* **2019,** *31* (14), e1807748-e1807748.
20. Witzigmann, D.; Hak, S.; van der Meel, R., Translating nanomedicines: Thinking beyond materials? A young investigator's reply to 'The Novelty Bubble'. *Journal of Controlled Release* **2018,** *290* (October), 138-140.
21. Trefts, E.; Gannon, M.; Wasserman, D. H., The liver. *Current Biology* **2017,** *27* (21), R1147-R1151.
22. Wisse, E., An electron microscopic study of the fenestrated endothelial lining of rat liver sinusoids. *Journal of Ultrastructure Research* **1970,** *31* (1), 125-150.
23. Braet, F.; Wisse, E., Structural and functional aspects of liver sinusoidal endothelial cell fenestrae: a review. *Comparative hepatology* **2002,** *1* (1), 1-1.
24. Smedsrod, B.; Pertoft, H.; Gustafson, S.; Laurent, T. C., Scavenger functions of the liver endothelial cell. *Biochem J* **1990,** *266* (2), 313-327.
25. Sørensen, K. K.; Simon-Santamaria, J.; McCuskey, R. S.; Smedsrød, B., Liver sinusoidal endothelial cells. *Comprehensive Physiology* **2015,** *5* (4), 1751-1774.
26. Poisson, J.; Lemoinne, S.; Boulanger, C.; Durand, F.; Moreau, R.; Valla, D.; Rautou, P. E., Liver sinusoidal endothelial cells: Physiology and role in liver diseases. *J Hepatol* **2017,** *66* (1), 212-227.
27. Diep, C. Q.; Ma, D.; Deo, R. C.; Holm, T. M.; Naylor, R. W.; Arora, N.; Wingert, R. A.; Bollig, F.; Djordjevic, G.; Lichman, B.; Zhu, H.; Ikenaga, T.; Ono, F.; Englert, C.; Cowan, C. A.; Hukriede, N. A.; Handin, R. I.; Davidson, A. J., Identification of adult nephron progenitors capable of kidney regeneration in zebrafish. *Nature* **2011,** *470* (7332), 95-100.
28. Smedsrod, B., Clearance function of scavenger endothelial cells. *Comp Hepatol* **2004,** *3 Suppl 1*, S22.
29. Ganesan, L. P.; Mohanty, S.; Kim, J.; Clark, K. R.; Robinson, J. M.; Anderson, C. L., Rapid and Efficient Clearance of Blood-borne Virus by Liver Sinusoidal Endothelium. *PLOS Pathogens* **2011,** *7* (9), e1002281-e1002281.
30. Mates, J. M.; Yao, Z.; Cheplowitz, A. M.; Suer, O.; Phillips, G. S.; Kwiek, J. J.; Rajaram, M. V. S.; Kim, J.; Robinson, J. M.; Ganesan, L. P.; Anderson, C. L., Mouse Liver Sinusoidal Endothelium Eliminates HIV-Like Particles from Blood at a Rate of 100 Million per Minute by a Second-Order Kinetic Process. 2017; Vol. 8, pp 35-35.
31. Sørensen, K. K.; McCourt, P.; Berg, T.; Crossley, C.; Couteur, D. L.; Wake, K.; Smedsrød, B., The scavenger endothelial cell: a new player in homeostasis and immunity. *American Journal of Physiology-Regulatory, Integrative and Comparative Physiology* **2012,** *303* (12), R1217-R1230.
32. Schledzewski, K.; Géraud, C.; Arnold, B.; Wang, S.; Gröne, H.-J.; Kempf, T.; Wollert, K. C.; Straub, B. K.; Schirmacher, P.; Demory, A.; Schönhaber, H.; Gratchev, A.; Dietz, L.; Thierse, H.-J.; Kzhyshkowska, J.; Goerdt, S., Deficiency of liver sinusoidal scavenger receptors stabilin-1 and -2 in mice causes glomerulofibrotic nephropathy via impaired hepatic clearance of noxious blood factors. *The Journal of Clinical Investigation* **2011,** *121* (2), 703-714.
33. McCourt, P. A. G.; Hansen, B.; Svistuonov, D.; Johansson, S.; Longati, P.; Schledzewski, K.; Kzhyshkowska, J.; Goerdt, S.; Johansson, S.; Smedsrød, B., The liver sinusoidal endothelial cell hyaluronan receptor and its homolog, stabilin-1 - Their roles (known and unknown) in endocytosis. *Comparative hepatology* **2004,** *3* (Suppl 1), S24-S24.
34. Wilkinson, A. L.; Qurashi, M.; Shetty, S., The Role of Sinusoidal Endothelial Cells in the Axis of Inflammation and Cancer Within the Liver. 2020; Vol. 11, pp 990-990.
35. Shetty, S.; Lalor, P. F.; Adams, D. H., Liver sinusoidal endothelial cells — gatekeepers of hepatic immunity. *Nature Reviews Gastroenterology & Hepatology* **2018,** *15* (9), 555-567.
36. Campbell, F.; Bos, F. L.; Sieber, S.; Arias-Alpizar, G.; Koch, B. E.; Huwyler, J.; Kros, A.; Bussmann, J., Directing Nanoparticle Biodistribution through Evasion and Exploitation of Stab2-Dependent Nanoparticle Uptake. *ACS Nano* **2018,** *12* (3), 2138-2150.
37. Sieber, S.; Grossen, P.; Bussmann, J.; Campbell, F.; Kros, A.; Witzigmann, D.; Huwyler, J., Zebrafish as a preclinical in vivo screening model for nanomedicines. *Advanced Drug Delivery Reviews* **2019,** *151-152*, 152-168.
38. Seternes, T.; Sørensen, K.; Smedsrød, B., Scavenger endothelial cells of vertebrates: a nonperipheral leukocyte system for high-capacity elimination of waste macromolecules. *Proceedings of the National Academy of Sciences of the United States of America* **2002,** *99* (11), 7594-7597.

39. Smedsrod, B., Scavenger function of liver sinusoidal endothelial cells. *The FASEB Journal* **2009,** *23* (S1), 66.61-66.61.
40. Hayashi, Y.; Takamiya, M.; Jensen, P. B.; Ojea-Jiménez, I.; Claude, H.; Antony, C.; Kjaer-Sorensen, K.; Grabher, C.; Boesen, T.; Gilliland, D.; Oxvig, C.; Strähle, U.; Weiss, C., Differential Nanoparticle Sequestration by Macrophages and Scavenger Endothelial Cells Visualized in Vivo in Real-Time and at Ultrastructural Resolution. *ACS Nano* **2020,** *14* (2), 1665-1681.
41. Evers, M. J. W.; Kulkarni, J. A.; Meel, R. V. D.; Cullis, P. R.; Vader, P.; Schiffelers, R. M., State-of-the-Art Design and Rapid-Mixing Production Techniques of Lipid Nanoparticles for Nucleic Acid Delivery. *Small methods* **2018,** *1700375*, 1-20.
42. Arteta, M. Y.; Kjellman, T.; Bartesaghi, S.; Wallin, S.; Wu, X.; Kvist, A. J.; Dabkowska, A.; Székely, N.; Radulescu, A.; Bergenholtz, J.; Lindfors, L., Successful reprogramming of cellular protein production through mRNA delivered by functionalized lipid nanoparticles. *Proceedings of the National Academy of Sciences of the United States of America* **2018,** *115* (15), E3351-E3360.
43. Yamamoto, T.; Ryan, R. O., Anionic phospholipids inhibit apolipoprotein E—Low-density lipoprotein receptor interactions. *Biochemical and Biophysical Research Communications* **2007,** *354* (3), 820-824.
44. Kulkarni, J. A.; Witzigmann, D.; Leung, J.; Tam, Y. Y. C.; Cullis, P. R., On the role of helper lipids in lipid nanoparticle formulations of siRNA. *Nanoscale* **2019,** *11* (45), 21733-21739.
45. Kulkarni, J. A.; Darjuan, M. M.; Mercer, J. E.; Chen, S.; van der Meel, R.; Thewalt, J. L.; Tam, Y. Y. C.; Cullis, P. R., On The Formation and Morphology of Lipid Nanoparticles Containing Ionizable Cationic Lipids and siRNA. *ACS Nano* **2018,** *12* (5), 4787-4795.
46. Leung, A. K. K.; Hafez, I. M.; Baoukina, S.; Belliveau, N. M.; Zhigaltsev, I. V.; Afshinmanesh, E.; Tieleman, D. P.; Hansen, C. L.; Hope, M. J.; Cullis, P. R., Lipid nanoparticles containing siRNA synthesized by microfluidic mixing exhibit an electron-dense nanostructured core. *Journal of Physical Chemistry C* **2012,** *116* (34), 18440-18450.
47. Kulkarni, J. A.; Witzigmann, D.; Leung, J.; van der Meel, R.; Zaifman, J.; Darjuan, M. M.; Grisch-Chan, H. M.; Thöny, B.; Tam, Y. Y. C.; Cullis, P. R., Fusion-dependent formation of lipid nanoparticles containing macromolecular payloads. *Nanoscale* **2019,** *11* (18), 9023-9031.
48. Crawford, R.; Dogdas, B.; Keough, E.; Haas, R. M.; Wepukhulu, W.; Krotzer, S.; Burke, P. A.; Sepp-Lorenzino, L.; Bagchi, A.; Howell, B. J., Analysis of lipid nanoparticles by Cryo-EM for characterizing siRNA delivery vehicles. *International journal of pharmaceutics* **2011,** *403* (1-2), 237-244.
49. Eygeris, Y.; Patel, S.; Jozic, A.; Sahay, G., Deconvoluting Lipid Nanoparticle Structure for Messenger RNA Delivery. *Nano Letters* **2020,** *20* (6), 4543-4549.
50. Patel, S.; Ashwanikumar, N.; Robinson, E.; Xia, Y.; Mihai, C.; Griffith, J. P.; Hou, S.; Esposito, A. A.; Ketova, T.; Welsher, K.; Joyal, J. L.; Almarsson, Ö.; Sahay, G., Naturally-occurring cholesterol analogues in lipid nanoparticles induce polymorphic shape and enhance intracellular delivery of mRNA. *Nature Communications* **2020,** *11* (1), 983-983.
51. Arias-Alpizar, G.; Koch, B.; Hamelmann, N. M.; Neustrup, M. A.; Paulusse, J. M. J.; Jiskoot, W.; Kros, A.; Bussmann, J., Stabilin-1 is required for the endothelial clearance of small anionic nanoparticles. *Nanomedicine* **2021,** *34*, 102395.
52. Reiser, A.; Woschée, D.; Mehrotra, N.; Krzysztoń, R.; Strey, H. H.; Rädler, J. O., Correlation of mRNA delivery timing and protein expression in lipid-based transfection. *Integrative Biology* **2019,** *11* (9), 362-371.
53. Balleza, E.; Kim, J. M.; Cluzel, P., Systematic characterization of maturation time of fluorescent proteins in living cells. *Nature Methods* **2018,** *15* (1), 47-51.
54. Lopes, S.; Yang, X.; Müller, J.; Carney, T.; McAdow, A.; Rauch, G.-J.; Jacoby, A.; Hurst, L.; Delfino-Machin, M.; Haffter, P.; Geisler, R.; Johnson, S.; Ward, A.; Kelsh, R., Leukocyte Tyrosine Kinase Functions in Pigment Cell Development. *PLoS genetics* **2008,** *4*, e1000026-e1000026.
55. Leonhardt, C.; Schwake, G.; Stögbauer, T. R.; Rappl, S.; Kuhr, J.-T.; Ligon, T. S.; Rädler, J. O., Single-cell mRNA transfection studies: Delivery, kinetics and statistics by numbers. *Nanomedicine: Nanotechnology, Biology and Medicine* **2014,** *10* (4), 679-688.
56. Patel, S.; Kim, J.; Herrera, M.; Mukherjee, A.; Kabanov, A. V.; Sahay, G., Brief update on endocytosis of nanomedicines. *Advanced Drug Delivery Reviews* **2019,** *144*, 90-111.
57. Gilleron, J.; Querbes, W.; Zeigerer, A.; Borodovsky, A.; Marsico, G.; Schubert, U.; Manygoats, K.; Seifert, S.; Andree, C.; Stöter, M., et al., Image-based analysis of lipid nanoparticle–mediated siRNA delivery, intracellular trafficking and endosomal escape. *Nature Biotechnology* **2013,** *31* (7), 638-646.

58. Sahay, G.; Querbes, W.; Alabi, C.; Eltoukhy, A.; Sarkar, S.; Zurenko, C.; Karagiannis, E.; Love, K.; Chen, D.; Zoncu, R.; Buganim, Y.; Schroeder, A.; Langer, R.; Anderson, D. G., Efficiency of siRNA delivery by lipid nanoparticles is limited by endocytic recycling. *Nature biotechnology* **2013,** *31* (7), 653-658.
59. Miller, C. M.; Donner, A. J.; Blank, E. E.; Egger, A. W.; Kellar, B. M.; Østergaard, M. E.; Seth, P. P.; Harris, E. N., Stabilin-1 and Stabilin-2 are specific receptors for the cellular internalization of phosphorothioate-modified antisense oligonucleotides (ASOs) in the liver. *Nucleic Acids Research* **2016,** *44* (6), 2782-2794.
60. Wilkins, B. J.; Pack, M., Zebrafish models of human liver development and disease. *Comprehensive Physiology* **2013,** *3* (3), 1213-1230.
61. Wang, S.; Miller, S. R.; Ober, E. A.; Sadler, K. C., Making It New Again: Insight Into Liver Development, Regeneration, and Disease From Zebrafish Research. *Current topics in developmental biology* **2017,** *124*, 161-195.
62. Korzh, S.; Pan, X.; Garcia-Lecea, M.; Winata, C. L.; Pan, X.; Wohland, T.; Korzh, V.; Gong, Z., Requirement of vasculogenesis and blood circulation in late stages of liver growth in zebrafish. *BMC developmental biology* **2008,** *8*, 84-84.
63. Mudumana, S. P.; Wan, H.; Singh, M.; Korzh, V.; Gong, Z., Expression analyses of zebrafish transferrin, ifabp, and elastaseB mRNAs as differentiation markers for the three major endodermal organs: liver, intestine, and exocrine pancreas. *Developmental dynamics : an official publication of the American Association of Anatomists* **2004,** *230* (1), 165-173.
64. Her, G. M.; Chiang, C.-C.; Chen, W.-Y.; Wu, J.-L., In vivo studies of liver-type fatty acid binding protein (L-FABP) gene expression in liver of transgenic zebrafish (Danio rerio). *FEBS letters* **2003,** *538* (1-3), 125-133.
65. Yin, C.; Evason, K. J.; Maher, J. J.; Stainier, D. Y. R., The basic helix-loop-helix transcription factor, heart and neural crest derivatives expressed transcript 2, marks hepatic stellate cells in zebrafish: analysis of stellate cell entry into the developing liver. *Hepatology (Baltimore, Md.)* **2012,** *56* (5), 1958-1970.
66. Cheng, D.; Morsch, M.; Shami, G. J.; Chung, R. S.; Braet, F., Albumin uptake and distribution in the zebrafish liver as observed via correlative imaging. *Experimental cell research* **2019,** *374* (1), 162-171.
67. Otis, J. P.; Zeituni, E. M.; Thierer, J. H.; Anderson, J. L.; Brown, A. C.; Boehm, E. D.; Cerchione, D. M.; Ceasrine, A. M.; Avraham-Davidi, I.; Tempelhof, H.; Yaniv, K.; Farber, S. A., Zebrafish as a model for apolipoprotein biology: comprehensive expression analysis and a role for ApoA-IV in regulating food intake. *Disease models & mechanisms* **2015,** *8* (3), 295-309.
68. Babin, P. J.; Thisse, C.; Durliat, M.; Andre, M.; Akimenko, M.-A.; Thisse, B., Both apolipoprotein E and A-I genes are present in a nonmammalian vertebrate and are highly expressed during embryonic development. *Proceedings of the National Academy of Sciences* **1997,** *94* (16), 8622 LP-8627.
69. Liu, C.; Kim, Y. S.; Kim, J.; Pattison, J.; Kamaid, A.; Miller, Y. I., Modeling hypercholesterolemia and vascular lipid accumulation in LDL receptor mutant zebrafish. *Journal of lipid research* **2018,** *59* (2), 391-399.
70. O'Hare, E. A.; Wang, X.; Montasser, M. E.; Chang, Y.-P. C.; Mitchell, B. D.; Zaghloul, N. A., Disruption of ldlr causes increased LDL-c and vascular lipid accumulation in a zebrafish model of hypercholesterolemia. *Journal of lipid research* **2014,** *55* (11), 2242-2253.
71. Schlegel, A., Zebrafish Models for Dyslipidemia and Atherosclerosis Research. 2016; Vol. 7, pp 159-159.
72. Wang, D.; El-Amouri, S. S.; Dai, M.; Kuan, C.-Y.; Hui, D. Y.; Brady, R. O.; Pan, D., Engineering a lysosomal enzyme with a derivative of receptor-binding domain of apoE enables delivery across the blood-brain barrier. *Proceedings of the National Academy of Sciences of the United States of America* **2013,** *110* (8), 2999-3004.
73. Jiang, Y.; Zhang, J.; Meng, F.; Zhong, Z., Apolipoprotein E Peptide-Directed Chimeric Polymersomes Mediate an Ultrahigh-Efficiency Targeted Protein Therapy for Glioblastoma. *ACS Nano* **2018,** *12* (11), 11070-11079.
74. Böckenhoff, A.; Cramer, S.; Wölte, P.; Knieling, S.; Wohlenberg, C.; Gieselmann, V.; Galla, H.-J.; Matzner, U., Comparison of five peptide vectors for improved brain delivery of the lysosomal enzyme arylsulfatase A. *The Journal of neuroscience : the official journal of the Society for Neuroscience* **2014,** *34* (9), 3122-3129.

75. Mayer, L. D.; Cullis, P. R.; Bally, M. B., Designing therapeutically optimized liposomal anticancer delivery systems: Lessons from conventional liposomes. Elsevier Science B.V.: Amsterdam, 1998; pp 231-257.
76. Sago, C. D.; Krupczak, B. R.; Lokugamage, M. P.; Gan, Z.; Dahlman, J. E., Cell Subtypes Within the Liver Microenvironment Differentially Interact with Lipid Nanoparticles. *Cellular and molecular bioengineering* **2019,** *12* (5), 389-397.
77. Shi, B.; Keough, E.; Matter, A.; Leander, K.; Young, S.; Carlini, E.; Sachs, A. B.; Tao, W.; Abrams, M.; Howell, B.; Sepp-Lorenzino, L., Biodistribution of small interfering RNA at the organ and cellular levels after lipid nanoparticle-mediated delivery. *The journal of histochemistry and cytochemistry : official journal of the Histochemistry Society* **2011,** *59* (8), 727-740.
78. Moderna Announces Positive Phase 1 Results for the First Systemic Messenger RNA Therapeutic Encoding a Secreted Protein (mRNA-1944). 2019.
79. Schulze, R. J.; Schott, M. B.; Casey, C. A.; Tuma, P. L.; McNiven, M. A., The cell biology of the hepatocyte: A membrane trafficking machine. *The Journal of cell biology* **2019,** *218* (7), 2096-2112.
80. Ni, Y.; Li, J.-M.; Liu, M.-K.; Zhang, T.-T.; Wang, D.-P.; Zhou, W.-H.; Hu, L.-Z.; Lv, W.-L., Pathological process of liver sinusoidal endothelial cells in liver diseases. *World journal of gastroenterology* **2017,** *23* (43), 7666-7677.
81. Rietwyk, S.; Peer, D., Next-Generation Lipids in RNA Interference Therapeutics. **2017,** *11* (8), 7572-7586.
82. Miao, L.; Li, L.; Huang, Y.; Delcassian, D.; Chahal, J.; Han, J.; Shi, Y.; Sadtler, K.; Gao, W.; Lin, J.; Doloff, J. C.; Langer, R.; Anderson, D. G., Delivery of mRNA vaccines with heterocyclic lipids increases anti-tumor efficacy by STING-mediated immune cell activation. *Nature Biotechnology* **2019,** *37* (10), 1174-1185.
83. Hassett, K. J.; Benenato, K. E.; Jacquinet, E.; Lee, A.; Woods, A.; Yuzhakov, O.; Himansu, S.; Deterling, J.; Geilich, B. M.; Ketova, T.; Mihai, C.; Lynn, A.; McFadyen, I.; Moore, M. J.; Senn, J. J.; Stanton, M. G.; Almarsson, Ö.; Ciaramella, G.; Brito, L. A., Optimization of Lipid Nanoparticles for Intramuscular Administration of mRNA Vaccines. *Molecular Therapy - Nucleic Acids* **2019,** *15* (April), 1-11.
84. Khvorova, A.; Watts, J. K., The chemical evolution of oligonucleotide therapies of clinical utility. *Nature Biotechnology* **2017,** *35* (3), 238-248.
85. Ku, S. H.; Jo, S. D.; Lee, Y. K.; Kim, K.; Kim, S. H., Chemical and structural modifications of RNAi therapeutics. *Advanced Drug Delivery Reviews* **2016,** *104*, 16-28.
86. Shen, X.; Corey, D. R., Chemistry, mechanism and clinical status of antisense oligonucleotides and duplex RNAs. *Nucleic Acids Research* **2017,** *46* (4), 1584-1600.
87. De Rijke, Y. B.; Biessen, E. A.; Vogelezang, C. J.; van Berkel, T. J., Binding characteristics of scavenger receptors on liver endothelial and Kupffer cells for modified low-density lipoproteins. *The Biochemical journal* **1994,** *304* (Pt 1), 69-73.
88. Cheng, Q.; Wei, T.; Farbiak, L.; Johnson, L. T.; Dilliard, S. A.; Siegwart, D. J., Selective organ targeting (SORT) nanoparticles for tissue-specific mRNA delivery and CRISPR–Cas gene editing. *Nature Nanotechnology* **2020,** *15* (4), 313-320.
89. Staudt, N.; Müller-Sienerth, N.; Fane-Dremucheva, A.; Yusaf, S. P.; Millrine, D.; Wright, G. J., A panel of recombinant monoclonal antibodies against zebrafish neural receptors and secreted proteins suitable for wholemount immunostaining. *Biochemical and biophysical research communications* **2015,** *456* (1), 527-533.
90. Burket, C. T.; Montgomery, J. E.; Thummel, R.; Kassen, S. C.; LaFave, M. C.; Langenau, D. M.; Zon, L. I.; Hyde, D. R., Generation and characterization of transgenic zebrafish lines using different ubiquitous promoters. *Transgenic research* **2008,** *17* (2), 265-279.
91. Varshney, G. K.; Pei, W.; LaFave, M. C.; Idol, J.; Xu, L.; Gallardo, V.; Carrington, B.; Bishop, K.; Jones, M.; Li, M.; Harper, U.; Huang, S. C.; Prakash, A.; Chen, W.; Sood, R.; Ledin, J.; Burgess, S. M., High-throughput gene targeting and phenotyping in zebrafish using CRISPR/Cas9. *Genome research* **2015,** *25* (7), 1030-1042.
92. Pardi, N.; Hogan, M. J.; Porter, F. W.; Weissman, D., mRNA vaccines — a new era in vaccinology. *Nature Reviews Drug Discovery* **2018,** *17* (4), 261-279.
93. John, S.; Yuzhakov, O.; Woods, A.; Deterling, J.; Hassett, K.; Shaw, C. A.; Ciaramella, G., Multi-antigenic human cytomegalovirus mRNA vaccines that elicit potent humoral and cell-mediated immunity. *Vaccine* **2018,** *36* (12), 1689-1699.

94. Zhang, N.-N.; Li, X.-F.; Deng, Y.-Q.; Zhao, H.; Huang, Y.-J.; Yang, G.; Huang, W.-J.; Gao, P.; Zhou, C.; Zhang, R.-R., et al., A Thermostable mRNA Vaccine against COVID-19. *Cell* **2020,** *182* (5), 1271-1283.e1216.
95. Jackson, L. A.; Anderson, E. J.; Rouphael, N. G.; Roberts, P. C.; Makhene, M.; Coler, R. N.; McCullough, M. P.; Chappell, J. D.; Denison, M. R.; Stevens, L. J., et al., An mRNA Vaccine against SARS-CoV-2 — Preliminary Report. *New England Journal of Medicine* **2020,** *383*, 1920-1931.
96. McKay, P. F.; Hu, K.; Blakney, A. K.; Samnuan, K.; Brown, J. C.; Penn, R.; Zhou, J.; Bouton, C. R.; Rogers, P.; Polra, K.; Lin, P. J. C.; Barbosa, C.; Tam, Y. K.; Barclay, W. S.; Shattock, R. J., Self-amplifying RNA SARS-CoV-2 lipid nanoparticle vaccine candidate induces high neutralizing antibody titers in mice. *Nature Communications* **2020,** *11* (1), 3523-3523.
97. Lu, J.; Lu, G.; Tan, S.; Xia, J.; Xiong, H.; Yu, X.; Qi, Q.; Yu, X.; Li, L.; Yu, H.; Xia, N.; Zhang, T.; Xu, Y.; Lin, J., A COVID-19 mRNA vaccine encoding SARS-CoV-2 virus-like particles induces a strong antiviral-like immune response in mice. *Cell Research* **2020,** *30* (10), 936-939.
98. Jain, R.; Frederick, J. P.; Huang, E. Y.; Burke, K. E.; Mauger, D. M.; Andrianova, E. A.; Farlow, S. J.; Siddiqui, S.; Pimentel, J.; Cheung-Ong, K.; McKinney, K. M.; Köhrer, C.; Moore, M. J.; Chakraborty, T., MicroRNAs Enable mRNA Therapeutics to Selectively Program Cancer Cells to Self-Destruct. *Nucleic acid therapeutics* **2018,** *28* (5), 285-296.
99. Jayaraman, M.; Ansell, S. M.; Mui, B. L.; Tam, Y. K.; Chen, J.; Du, X.; Butler, D.; Eltepu, L.; Matsuda, S.; Narayanannair, J. K.; Rajeev, K. G.; Hafez, I. M.; Akinc, A.; Maier, M. A.; Tracy, M. A.; Cullis, P. R.; Madden, T. D.; Manoharan, M.; Hope, M. J., Maximizing the potency of siRNA lipid nanoparticles for hepatic gene silencing in vivo. *Angew Chem Int Ed Engl* **2012,** *51* (34), 8529-8533.
100. Sun, Q.; Cai, S.; Peterson, B. R., Practical synthesis of 3beta-amino-5-cholestene and related 3beta-halides involving i-steroid and retro-i-steroid rearrangements. *Org Lett* **2009,** *11* (3), 567-570.
101. Schindelin, J.; Arganda-Carreras, I.; Frise, E.; Kaynig, V.; Longair, M.; Pietzsch, T.; Preibisch, S.; Rueden, C.; Saalfeld, S.; Schmid, B.; Tinevez, J. Y.; White, D. J.; Hartenstein, V.; Eliceiri, K.; Tomancak, P.; Cardona, A., Fiji: an open-source platform for biological-image analysis. *Nat Methods* **2012,** *9* (7), 676-682.
102. Ellett, F.; Pase, L.; Hayman, J. W.; Andrianopoulos, A.; Lieschke, G. J., mpeg1 promoter transgenes direct macrophage-lineage expression in zebrafish. *Blood* **2011,** *117* (4), e49-56.
103. Weinstein, B. M.; Stemple, D. L.; Driever, W.; Fishman, M. C., Gridlock, a localized heritable vascular patterning defect in the zebrafish. *Nat Med* **1995,** *1* (11), 1143-1147.
104. Severgnini, M.; Sherman, J.; Sehgal, A.; Jayaprakash, N. K.; Aubin, J.; Wang, G.; Zhang, L.; Peng, C. G.; Yucius, K.; Butler, J.; Fitzgerald, K., A rapid two-step method for isolation of functional primary mouse hepatocytes: cell characterization and asialoglycoprotein receptor based assay development. *Cytotechnology* **2012,** *64* (2), 187-195.